SYNTHESIS AND CHARACTERIZATION OF LITHIUM SILICATE CERAMIC FOR THE TEST BLANKET MODULE (TBM) IN FUSION REACTORS

A Thesis Submitted in Partial Fulfillment of the Requirements for the Degree of

MASTER OF TECHNOLOGY(RESEARCH)

by

ABHISEK CHOUDHARY
(Roll No: 609CR601)

Under the Guidance of

Prof. Ranabrata Mazumder

and

Prof. Santanu Bhattacharyya

DEPARTMENT OF CERAMIC ENGINEERING

NATIONAL INSTITUTE OF TECHNOLOGY, ROURKELA

2012

NATIONAL INSTITUTE OF TECHNOLOGY

Rourkela, INDIA

CERTIFICATE

This is to certify that the thesis entitled **"SYNTHESIS AND CHARACTERIZATION OF LITHIUM SILICATE CERAMIC FOR THE TEST BLANKET MODULE (TBM) IN FUSION REACTORS"** beingsubmitted by **Mr. Abhisek Choudhary**, for the degree of **Master of Technology** (Research) **in Ceramic Engineering** to the National Institute of Technology, Rourkela, is a record of bonafide research work carried out by him under our supervision and guidance. His thesis, in our opinion, is worthy of consideration for the award of degree of Master of Technology (Research) in accordance with the regulations of the institute.

The results embodied in this thesis have not been submitted to any other university or institute for the award of a Degree.

Dr. R. Mazumder
Associate Professor
Department of Ceramic Engineering
National Institute of Technology, Rourkela

Dr. S. Bhattacharyya
Professor
Department of Ceramic Engineering
National Institute of Technology, Rourkela

CONTENTS

4. Experimental Work

5. Results and Discussion

Acknowledgements

This dissertation would not have been possible without the guidance and the help of several individuals who in one way or another contributed and extended their valuable assistance in the preparation and completion of this study.

Foremost, I would like to express my sincere gratitude to my advisors Prof. Ranabrata Mazumder and Prof. Santanu Bhattacharyya for the continuous support of my M.Tech(R) study and research, for their patience, motivation, enthusiasm, and immense knowledge. I attribute the level of my Master's degree to their encouragement and effort and without them this thesis, too, would not have been completed or written. One simply could not wish for better or friendlier supervisors.

I am extremely thankful to Board of Research for Fusion Science and Technology **(BRFST)**and our collaborating Institute i.e. Institute of Plasma Research **(IPR)** for providing me the financial support throughout my research period.

I express my sincere thanks to Prof. Swadesh Pratihar, Head, Ceramic Engineering for providing me all the departmental facilities required for the completion of the thesis. His out of the way help and guidance helped the thesis to reach the final shape. I am also thankful to all other faculty members of Ceramic Engineering Department, NIT Rourkela for their invaluable advice, constant help, encouragement, inspiration and blessings.

I am grateful to Director,CGCRI,Kolkata for permitting me to carry out the ICP-AES analysis and thermal conductivity measurements at their Institute.

I am also indebted to my senior research colleagues Yugo bhai, Nadiya bhai, Sarat bhai, Subrat Bhai, Ganesh Bhai and Sanjay bhai for their unconditional support and constant motivation whenever needed. I am very grateful to all my dear friends Bhabani, Gita, Pramita, Sabya, James who have given me their friendship, put up with my odd hours, and provided me with lifts and practical help.Last but not the least, I would like to thank my dear parents, brother and sisters (Ranu, romi and lucy) for their support.

Abhisek Choudhary

Abstract

Lithium-based ceramic, Li_4SiO_4, is being considered as promising solid breeder materials in the tritium breeding blanket of thermonuclear fusion reactors, because of its high Li- density, high thermal conductivity and prominent tritium release rate at low temperatures between 300 and 500^oC, its low activation characteristics, low thermal expansion coefficient and high thermal conductivity. For tritium recovery purpose samples having 85-90% of true density with open porosity (around 5%) is required. Uniform small grain size distribution (having diameter between 2-4μm) is preferable as activation energy for tritium diffusion through grain is higher compared to grain boundary. Solid state method requires higher calcination temperature, producing coarser particle and impurity, which adversely affects in achieving high sintered density (above 85% of theoretical density) and forms large grain size with entrapped closed pore inside the grain.

In the current work Li_4SiO_4 powder was synthesized by solution combustion technique using cheaper precursor of silica i.e. from rice husk ash (an agricultural waste). We found that by controlling the metal to citrate ratio of the solution and calcination temperature of the as-burnt powder phase purity can be achieved. The particle size of Li_4SiO_4 powder (prepared at M/C=1.4) was found to be 100-200 nm with low surface area ($2m^2/gm$). It was found that Li_4SiO_4 powder can be sintered at a temperature as low as 900^oC with a density ~ 85% of the theoretical density. Phase stability in the sintered sample was studied. Attempts were made to minimize the lithium loss from the sintered specimens. Moisture reactivity studies were conducted together with FTIR spectroscopy on calcined powder to find out the moisture affinity of the samples. Kinetics of the initial stage of sintering from the shrinkage data has been analyzed to find out the sintering mechanism. Thermal diffusivity measured by laser flash method. Thermal conductivity value depends on the density of the sample. AC impedance method has been used to characterize electrical property of the sintered sample as tritium diffusion is related to the Li^+ ion conductivity in Li_4SiO_4.

Keywords: Lithium orthosilicate, sintering, thermal conductivity, electrical conductivity

List of figures

List of tables

Chapter 1

Introduction

1.1 Current world energy scenario

The use of energy is proportional to living standard of the human society. With high standard of livingand development of society, the energy requirement has increased in every aspect of daily life like food, heating, lighting, transportation etc. At present, we are still dependent on non-renewable fossil fuels like Coal, Natural gases and Oils, which are actually polluting the environment by giving out the greenhouse gases. Moreover the studies show that the reserve of these fossil fuels will be consumed in coming few decades. Fig. 1.1 shows relative percentage of primary energy sources for global energy usage in 2011. It is clear that more than 80% of the energy comes from Oil, Coal and Natural gases, which are non-renewable and non-environmentfriendly. So the need of the hour is to look at alternative options for the energy sources**.**The energy given by sun per minute equals the world's energy demand per year.But our available technology lacks to absorb all these solar energy and to convert it into the useful one. For example the photovoltaic (solar) cell converts the solar energy directly in to the electricity. But the high manufacturing cost and low energy conversion efficiency limits its use [1]. Likewise, the usage of other energy sources like wind, geothermal and others are limited due to one or another reason.

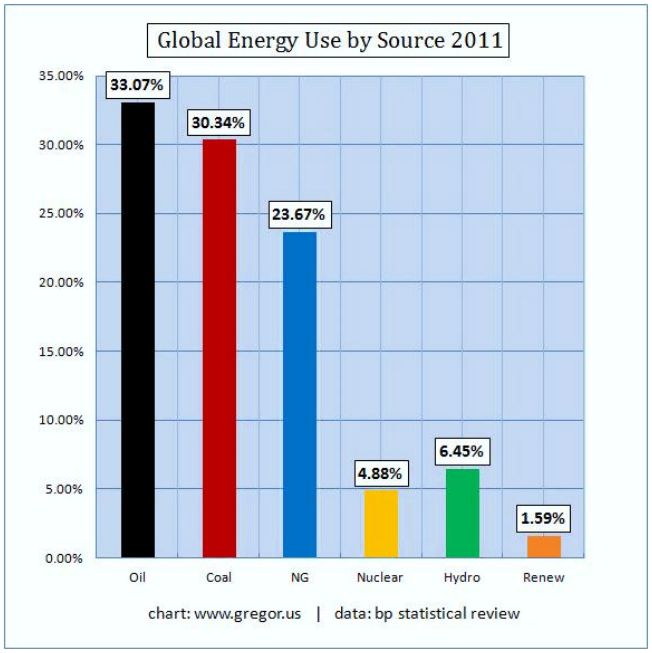

Fig.1.1 World energy usage in 2011(Image source: www.gregor.us)

We are quite familiar with the Nuclear Fission and Fusion Energy, which are the two ways to get nuclear energy according to the well-known binding energy curve and Einstein's well known mass-energy relation [2],[3]. Currentlyall the nuclear energy that we usecomes from nuclear fission, in which splitting of heavy nucleus such as U-235 occurs in two lighter nuclei with the release of enormous energy. But fission technology has got its own problems related to safety issues and radioactive waste management. On the other hand fusion process is merging of two light nuclei and resulting in a heavier nuclei plus energy. Fig. 1.2 shows binding energy release in both processes.It is seen that the fusion reaction releases much higher energies than fission reactions. Moreover that, the radioactive waste from fusion devices is expected very less in amount and relatively very short half lifetime compare to fission [4].Sun energy, that we are using and on which whole life cycle based, is one best example of fusion occurring naturally.

1.2 Physics behind nuclear fusion

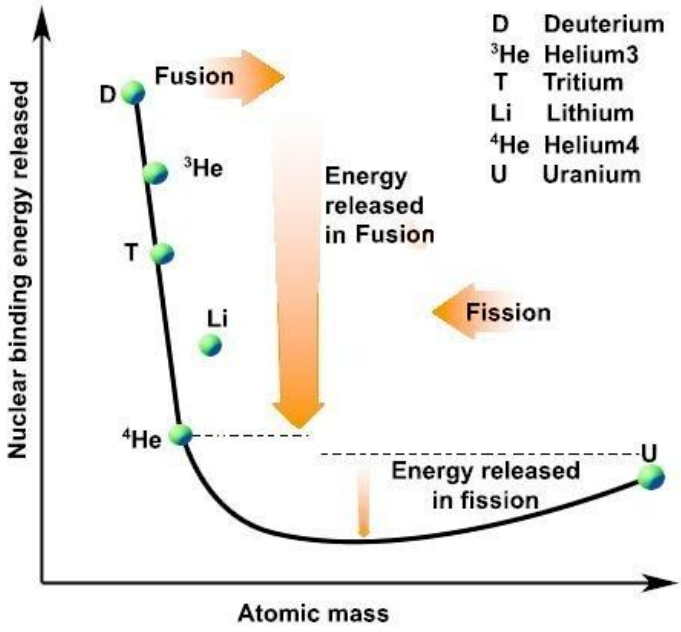

Fig. 1.2 Nuclear binding energy per nucleon as a function of the atomic mass A
(Image source:Hydrocarbon catalytic nuclear fusion by using quantum spin hall effect, *SiemensStudentaward*- middleeast, idea:246,(2011))

For fusion of two positively charged nuclei, one has to overcome the long range Coulombic forces. Once the nuclei reach to the range of distance at which the strong short range nuclear forces comes in the action the fusion reaction occurs. The Coulombic potential energy between two charges, say ‘a’ and ‘b’, is given by the formula,

$$V_{ab} = \frac{1}{4\pi\varepsilon}\frac{ab}{r_m} \qquad (1.1)$$

Where r_m is the distance at which the strong nuclear forces come in action,

for example $r_m \approx 5 \times 10^{-15}$ for D-T fusion reaction and therefore the potential energy will be V = 280 keV, It means that we have to heat the plasma approximately 3000 million ^{o}C. But in reality quantum effect reduces the requirement of such high temperature allowing the fusion reaction at well below temperatures 150 million ^{o}C (15 keV) [5]. A schematic representation of the potential energy of two nuclei as a function of their distance is shown in Fig. 1.3.

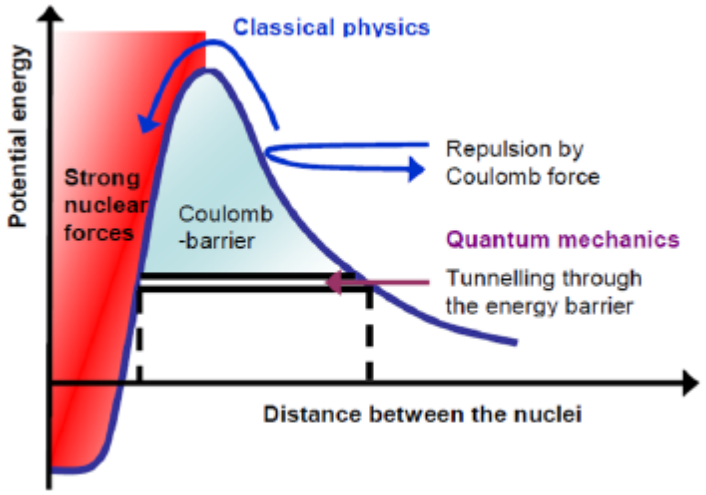

Fig. 1.3 Schematic representation of the potential energy of two nuclei as a function of their distances

(Image source:M.Decreton, V.Massaut, I.Uytdenhouwen, J.Braet, F.Druyts ,B.Brichard and E.Laes, Report at Belgian Nuclear Institute SCK-CEN, Mol (2007)

An example of uncontrolled fusion reaction has been conducted by the United States long back in 1952 through hydrogen bomb test. But this way of nuclear energy production was not a controlled one and hence was not of direct use to the mankind for a peaceful energy production. Scientists realized that it is necessary to confine this hot gas by means of some external forces. For example gravitational force of sun helps to confine the charged particles and allows fusion reaction to take place on the sun. But for laboratory purpose, fusion reaction occurs at very small dimensions where gravity doesn't play any major role at all. Behaviour of charged particles in magnetic field lead to the idea of linear devices (Magnetic Mirrors), but with high kinetic energy of these charged particles the confinement was poor (loss of energetic particles). In order to overcome this problem, the linear devices replaced by a torus, in which the charged particle ideally would have their path infinite long.

1.3 Fusion reaction of deuterium and tritium

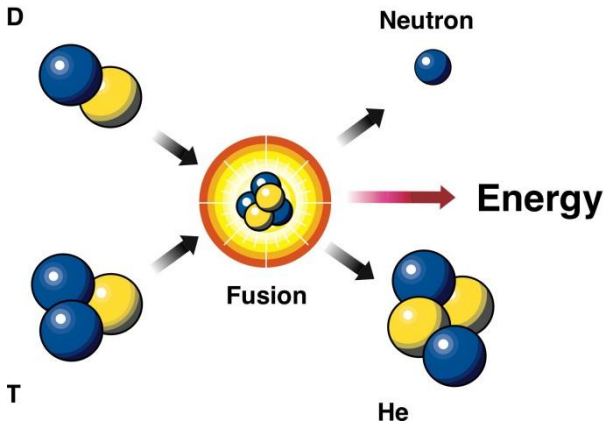

Fig. 1.4 Fusion reaction of deuterium and tritium (Image source: Arthur Beiser 6th Edition ,Tata McGraw-Hill Edition,(2002)

$$ {}_1^2D + {}_1^3T \rightarrow {}_2^4He(3.5MeV) + n^0(14.1MeV) \qquad (1.2) $$

In the above equation 1.2, D stands for Deuterium and T stands for Tritium, both are isotopes of Hydrogen. The D-T reaction produces charge-less energetic neutrons, each with enormous energy of 14.1 MeV. This is the main reason for energy production by the nuclear reactor. In a fusion reactor the required fusion fuel will be only of the order of few grams (continuously refilled) which is one positive side of fusion fuel compare with the quantity required in tones to produce the same amount of energy. And the output will be harm-less inert gas Helium. If we look at sources for fusion fuel, deuterium occurs naturally in the sea water which can be extracted easily at very low cost. And tritium is a radioactive isotope of hydrogen with half life time of about 12.3 years. Tritium doesn't occur naturally on earth but one can produce it from breeding of lithium. Lithium has three protons in its nucleus and exists in two forms—one with three neutrons, known as *lithium-6* , and one with four neutrons, known as *lithium-7*.Both forms interact with neutrons to produce tritium and helium. In the firstreaction energy is released, but energy has to be put into the second reaction (eqn 1.3 & 1.4).Thus isotope ^{6}Li, which is available in enough quantity on the earth, to be used to provide necessary energy for next few hundreds of years. Thus fusion power could provide a major contribution to a future clean and sustainable energy mix for society.

$$ {}_3^6\mathrm{Li} + \mathrm{n} \rightarrow \mathrm{T} + {}_2^4\mathrm{He} + 4.8\mathrm{Mev} \qquad (1.3) $$

$$ {}_3^7\mathrm{Li} + \mathrm{n} \rightarrow \mathrm{T} + \mathrm{n} + {}_2^4\mathrm{He} - 2.5\mathrm{Mev} \qquad (1.4) $$

1.4 Why is Lithium required for tritium breeding?

Lithium has been identified as the only viable element to breed Tritium.Naturally occurring lithium is composed of two stable isotopes,^{6}Li and ^{7}Li, the latter being the more abundant (92.5% natural abundance). Both natural isotopes of Lithium have exceptionally low nuclear binding energy per nucleon compared to the next lighter and heavier elements, helium and beryllium. Thus, Lithium is among the stable light element.For atoms with low atomic numbers, a nucleus that has a different number of protons than neutrons can potentially drop to a lower energy state through a radioactive decay that causes the number of protons and neutrons to matchclosely. The neutron and the proton are different types of fermions. The Pauli Exclusion Principle is a quantum mechanical effect that prohibits identical fermions, such as multiple protons, from occupying the same quantum physical state at the same time. Thus every proton in the nucleus must occupy a different state, with its own energy level, and the same rule applies to all of the neutrons. This prohibition does not apply to a proton and neutron occupying the same quantum state. Since lithium^{7}Li has an extra neutron in its atomic nuclei, a lower value of proton to neutron ratio its binding energy to be low. This makes Lithium a suitable candidate for tritium breeding than any other element.

1.5 Lithium bearing ceramics for tritium production

Interest in the use of solid lithium-based materials as tritium breeders for fusion blankets has grown since the late 1970s. Ceramic lithium compounds are used as breeder for fusion blanket because of more favorable physical characteristics for the severe operating conditions of high temperatures and intense neutron fluxes. Lithium-containing ceramics such as Li_2O, γ-$LiAlO_2$, Li_4SiO_4, Li_2ZrO_3 and Li_2TiO_3 have been considered as candidates for tritium breeding materials in D–T fusion reactors of the ITER test blanket module (TBM) for DEMO reactor [6]-[11]. The tritium breeder blanket in the fusion reactor serves three primary functions (as shown in fig 1.5):

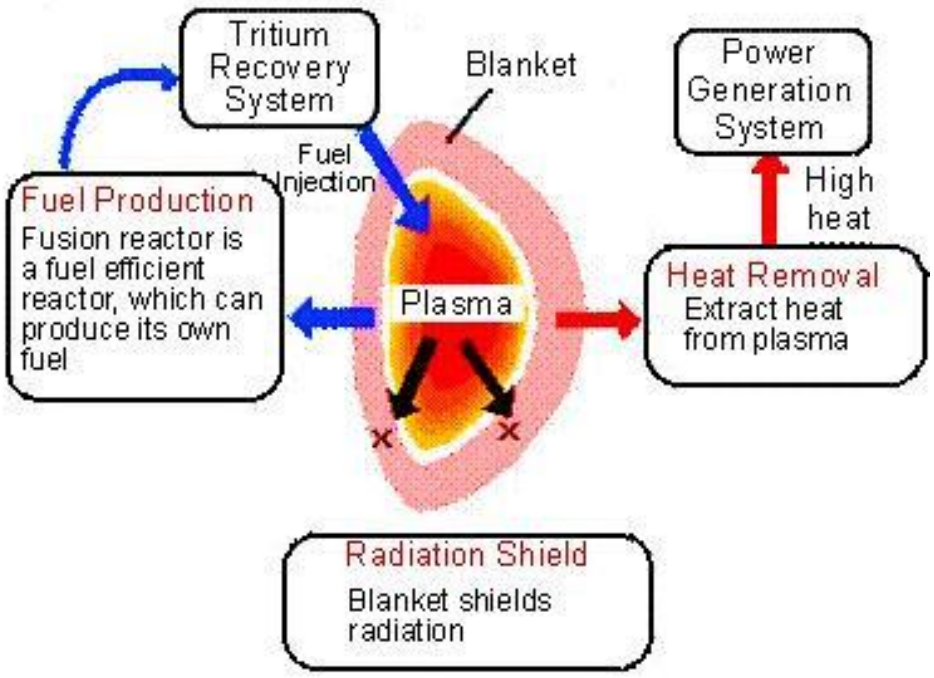

Fig. 1.5 Roles of blanket (Image source:www.naka.jaea.go.jp)

(a) **Tritium Breeding** - To produce and recover all tritium;

(b) **Heat Extraction** - Converting the released energy into sensible heat;

(c) **Radiation Shield** - Shielding from neutron & gamma radiation.

The above points are critical for the fusion power development.Since fusion blanket extract heat and produce fusion fuel, it is regarded as a key component of a fusion plant.Principal requirements to be fulfilled by the breeder material are

(i) Breeding and releasing of tritium,

(ii) Physical and chemical stability at high temperature,

(iii) Compatibility with other blanket components, and

(iv) Possessing adequate irradiation behavior.

On the basis of their overall desirable properties, lithium-containing ceramics are recognized as attractive tritium breeding materials for fusion reactor blankets [12]-[13].

1.6 Function of the tritium breeder in Test blanket Module (TBM)

DEMO and ITER:

DEMO is the demonstration reactor which is going to be constructed and tested before the actual realization of ITER (International Thermonuclear Experimental Reactor) which may produceelectrical power. In order to achieve this in the shortest timescale, studies have shown that, a parallel programme of materials testing over and above that of ITER would be needed. In particular, DEMO will rely on a "hot breeding blanket" to convert the kinetic energy of the neutrons created in the plasma chamber into heat [14].

A Test Blanket Module (TBM) comprises lithium ceramics as breeder material, beryllium as neutron multiplier, helium as coolant, and martensitic steel as structural material. The lithium breeder is impounded upon the structural material to form the blanket. The blanket differs essentially by the architecture of their cooling system. The various DEMO solid breeding blankets considered by ITER parties are:

a) Helium Cooled Ceramic Breeder (HCCB)
b) Water Cooled Ceramic Breeder (WCCB)

Both HCCB and WCCB concepts are similar, in the use of their structural materials, multiplier and ceramic breeder, with the later concept considered only by Japan.

Indeed the production of one tritium atom by the $^{6}Li(n, \alpha)T$ reaction (Eqn.1.3) consumes one neutron, while its fusion with a deuterium (Eqn.1.2) generates only one neutron which exhibits a significant probability (30-35%) of not being available for tritium production (because of parasitic absorptions in blanket structures, or streaming through the blanket opening). These neutron losses must therefore be compensated. Hence a neutron multiplier (beryllium or lead) is incorporated in the blanket, in addition to a ^{6}Li-rich compound.

Fig.1.6 shows the schematic diagram of ITER device along with TBM and Ceramic Breeders. TBM has two crucial functions. Firstly, it produces and recovers all tritium produced from the DT reaction (Eqn.1.2) and secondly acts as a heat exchanger i.e. extracts heat from plasma and supplies it to the power generation system.

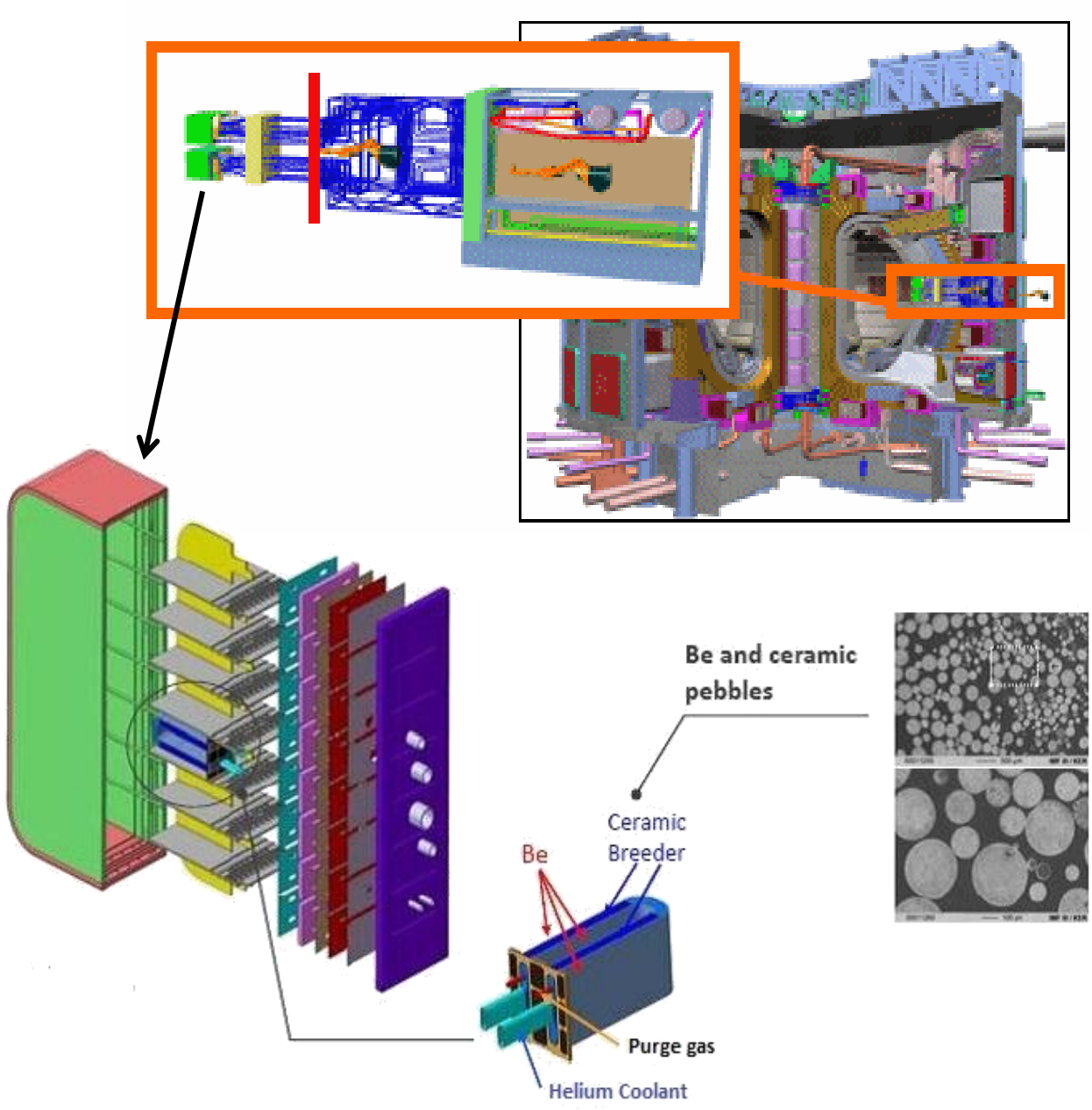

Fig. 1.6 Schematic diagram of ITER along with TBM and Ceramic Breeder Ports

(Image source: www.fuziotech.hu and www.kit.edu)

1.7 Different kinds of breeder materials and their properties

Among various properties of breeder materials, physical and thermal, mechanical, chemical stability and compatibility, tritium solubility and transport, irradiation effects, thermal cycling effects, waste disposal and other miscellaneous properties of breeding materials are very much important.Lithium contained ceramics such as Li_2O, γ-$LiAlO_2$, Li_4SiO_4, Li_2ZrO_3 and $Li_2TiO_3$are recently considered as candidates for tritium breeding materials in D–T fusion reactors of the ITER test blanket module (TBM) for DEMO reactor [15]-[19].

Lithium Oxide (Li_2O):

Lithium oxide (Li_2O) is an attractive ceramic breeder material because of its highest lithium atom density (0.94 g/cc)among all the lithium based breeder ceramicsfor tritium breeding. Li_2O has high thermal conductivity, good tritium release properties and low activation. Li_2O is considered to be the only ceramic candidate among Li_2TiO_3, Li_2ZrO_3 and Li_4SiO_4 for achieving the Tritium Breeding Ratio (TBR) larger than unity in absence of a neutron multiplier.However, at temperatures below a moisture-pressure-dependent critical value (e.g., 366°C at 10 Pa), LiOH will precipitate out as a separate phase, thereby increasing tritium retention to unacceptable levels. This results in transport of Lithium to cooler zones of Breeding Blanket which in turn contributes to the lithium loss from the blanket. At high temperatures (e.g., 800-1000°C), transport of vapor phase of LiOH, as well as chemical incompatibility with structural materials, may cause design problems. Measurements made using a carrier gas stream of varying H_2O partial pressure showed that moisture enhances the volatility of Li_2O as LiOH [20]. Thus, controlling moisture pressure is essential to Li_2O performance.

Lithium Aluminate ($LiAlO_2$):

$LiAlO_2$exist in three allotropic forms viz.α, β, and γ - $LiAlO_2$ which are hexagonal, monoclinic, and tetragonal, respectively.Out of which γ - $LiAlO_2$is a tritium breeder material. γ - $LiAlO_2$possesses lowest lithium atom density of about 0.27 g/cc for which little interest is given in this lithium based ceramics. Lithium aluminate may be better than Li_2O in terms of its higher melting temperature and better swelling resistance.Swelling of lithium based

ceramics leads to reduction of the pressure of purge gas. $LiAlO_2$ has broader operating temperature (450- 1200^oC) with excellent irradiation behavior. However it requires a higher minimum operating temperature to maintain low tritiuminventory. Effective neutron multiplier is required for adequate tritium breeding.The Tritium release characteristics are also poor [21].

Lithium Zirconate (Li_2ZrO_3) :

Li_2ZrO_3 has second lowest Lithium atom density (0.33 g/cc) among the various Lithium based ceramics. It is not as attractive asLi_2O with regard to tritium breeding, heat transport and activation.It also exhibits lowest tritium retention at low operating temperatures (400-1400^oC) [21].Its compatibility with structural materials is just as good as the other ternaries (Li_4SiO_4 and $LiAlO_3$) and much better than that of Li_2O.Li_2ZrO_3 has long-term radioactive characteristics than Li_2O, Li_4SiO_4**,** and Li_2TiO_3.$Li_2ZrO_3$is thermodynamically unstable against water vapor at room temperature [22]. Li_2ZrO_3also shows large thermal anomalies in the thermal properties from 225 to 625^oC. The anomalies may be due to anisotropy in the thermal expansion of the monoclinic crystal [23].

Lithium Titanate (Li_2TiO_3):

Li_2TiO_3 is a low-activation ceramic material for use in tritium breeding.The lithium atom density of $Li_2TiO_3$is also better than $Li_2ZrO_3$and $LiAlO_2$(0.43g/cc).It has got better thermal conductivity as well high thermal stabilitythan $Li_2ZrO_3$and $LiAlO_2$. Its long term waste problem is also low because titanium is a low activation element. Its moisture reactivity is less when compared to other breeder ceramics. Li_2TiO_3 shows good compatibility with structural materials.It has got good tritium release properties at low temperature i.e between 200 – 400^oC [16]-[20].

Lithium Orthosilicate (Li_4SiO_4):

Li_4SiO_4 possesses the second best lithium atom density i.e. next to Li_2O (0.54 g/cc). It exhibits the most favorable tritium release behavior.Li_4SiO_4 does not produce long-lived activation products during the irradiation process. It has got little moisture affinity which can be controlled if proper arrangements are made. Its thermal conductivity is better than other

Lithium based solid breeder materials i.e. only next to Li_2O. The swelling resistance and thermal expansion of $Li_4SiO_4$is also quite low. It is compatible with other blanket and structural materials[24]-[28]. The working temperature is quite similar to that of Li_2TiO_3.

1.8 Summary

It is seen that the lithium atom density plays a major role on TBR. Higher the lithium atom density better will be the TBR. So, in this respect Li_2O is the best but due to its higher reactivity with water it is not considered as an attractive option. Thus, the second best Li_4SiO_4 is considered. However, TBR factor is not as critical as thought, since there is evidence that we have to use Beryllium neutron multiplier and ^6Li enrichment for achieving TBR > 1 [12]. The thermo mechanical and thermochemical stability of lithium ceramics is important from safety considerations. The thermal properties like thermal conductivity and thermal expansion of breeder materials are very crucial from the point of view of heat conduction and subsequent tritium release. In this context, Li_2O also possesses highest thermal conductivity value but due to its problem Li_4SiO_4(Thermal conductivity just below that of Li_2O) is a promising breeder material [29].Thermal conductivity values for various lithium based materials can be arranged as follows:

$$Li_2O > Li_4SiO_4 > Li_2TiO_3 > Li_2ZrO_3 > \gamma - LiAlO_2$$ [30].

The moisture uptake and neutron activation are important feature of breeder material. Although $Li_2ZrO_3$and $Li_2TiO_3$are similar in properties, we see that moisture uptake and neutron activation are lower in titanate. This makes Li_2TiO_3a better breeder material than Li_2ZrO_3.With increase in lithium atom density of the lithium based ceramics, the vapor pressure of lithium increases. High lithium vapor pressure is undesirable from the point of view of tritium transport[32].Li_2O exhibited the largest linear thermal expansion, while y-$LiAlO_2$ and Li_2ZrO_3 showed the least expansion. The thermal expansion value of Li_4SiO_4 is lower than Li_2O [33]. Therefore it is better to concentrate more on ternary ceramics because Li_2O is more chemically active, exhibiting more compatibility problems with structural and breeder materials, more swelling when subjected to neutron irradiation [34].

Vaporization behavior for several candidate breeder materials is an important property from the point of view of design of tritium breeding blanket. Authors have measured the vapor

pressure over the lithium ceramics as a function of temperature, in vacuum.The order for increasing lithium oxide vapor pressures is as follows [35]:

$$LiAlO_2 < Li_2TiO_3 < Li_2ZrO_3 < Li_4SiO_4 < Li_2O$$

Thus, overall properties of Li_4SiO_4(Thermal conductivity, Lithium atom density etc.) is better than other lithium-based ceramics which makes it one of the promising tritium breeder material.

References

[1] H.J.MollerC.FunkeM.Rinio and S.Scholz, Thin Solid Films **487** (2005)179.

[2] J. G. Linhart, Plasma Physics (North-Holland Publishing Company, Amsterdam, 1960).

[3] I. Kaplan, Nuclear Physics (Addison-Wesley Pub. Co., London, 1964).

[4] J. Ongena and G. Van Oost, Trans. of Fus. Sci. Tech.**49**(2006)3.

[5] G. McCracken and P. Stott, Fusion - The Energy of the Universe (Elsevier AcademicPress, UK, 2005).

[6] C.E. Johnson, G.W. Hollenberg, N. Roux, H. Watanabe,Fusion Eng. Des. **8** (1989) 145.

[7] N. Roux, J. Avon , A. Floreancig , J. Mougin, B. Rasneur, S. Ravel,J.Nucl.Mater.**233-237** (1996) 1431.

[8] J.D.Lulewicz, N. Roux, Fusion Eng. Des.**39–40** (1998) 745.

[9] X.Wu, Z. Wen, X.Xu, Z. Gu, X.Xu, J.Nucl. Mater.**373** (2008) 206.

[10] C.E. Johnson, Cer. Inter.**17** (1991) 253.

[11] C.E. Johnson, J.Nucl. Mater.**270** (1999) 212.

[12] N. Roux, G. Hollenberg, C. Johnson, K. Noda, R.Verrall, Fusion Eng. Des. **27** (1995) 154.

[13] G. Piazza, J. Reimann, E. Günther, R. Knitter, N. Roux, J.D. Lulewicz, J. Nucl. Mater. **307–311** (2002) 811.

[14] E. Proust, L. Anzidei, G. Casini, M. Dalle Donne, L. Giancarli and S. Malang ,Fusion Eng. Des.**22** (1993) 19.

[15] L.M. Lidsky, Nucl. Fusion **15** (1975) 151.

[16] N. Roux, S. Tanaka, C. Johnson, R. Verrall, Fusion Eng. Des.**41** (1998) 31.

[17] P. Gierszewski, Fusion Eng. Des.**39–40** (1998) 739.

[18] J.M. Miller, H.B. Hamilton, J.D. Sullivan, J. Nucl.Mater. **212–215** (1994) 877.

[19] J.P. Kopasz, J.M. Miller, C.E. Johnson, J. Nucl. Mater. **212-215** (1994) 927.

[20] M. Tetenbaum and C.E. Johnson, J. Nucl. Mater. **120**(1984) 213.

[21] C. E. Johnson,K. R. Kummerer, E. Roth,J.Nucl. Mater. **155-157** (1988) 188.

[22] Y.Zou and A.Petric, J. Phys. Chem. Solids**6**. (1994) 493.

[23] Y. Takahashi, T. Ohsato and T. Terai,Fusion Eng. Des.**17** (1991) 25.

[24] J. Charpin, F. Botter, M.Briec, B. Rasneur, E. Roth, N. Roux, J. Sannier, Fusion Eng. Des. **8** (1989) 407.

[25] C.E. Johnson, R.G. Clemmer, J. Nucl. Mater. **103&104**(1981) 547.

[26] Y. Liu, M.C. Hollenberg, Fusion Technol. **8** (1985)1970.

[27] C.E. Johnson, K.R. Kummerer, E. Roth, J. Nucl. Mater.**155-157** (1988) 188.

[28] J. Jimenez-Becerril, P. Bosch, S. Bulbulian, J. Nucl. Mater.**185** (1991) 304.

[29] A. Abou-Sena, A. Ying, and M. Abdou, Fusion Sci. Tech.**47** (2005) 1094.

[30] J.W. Davis, A.A. Haasz, J. Nucl. Mater. **232**{15**}**(1996) 65.

[31] D. J. Suiter, J. W. Davis, B. A. Kirkpatrick,J. Nucl. Mater.**103 & 104** (1981) 579.

[32] H.R. Ihle, R.D. Penzhorn and P. Schuster J. Nucl. Mater. **155-157** (1988) 471.

[33] D.L. Smith, Blanket Comparison and Selection Study, ANL/FPP84-1, **2** (1984) Ch-6.3.

[34] G.W. Hollenberg and D.L. Baldwin, J. Nucl. Mater. **133-134** (1985) 242.

[35] M. Asano, Y. Kato, T. Harada, Y. Mizutani, CBBI-4, Kyoto, (1995).

Chapter 2

Literature Review

2.1 Phase diagram of Li_2O-SiO_2 system

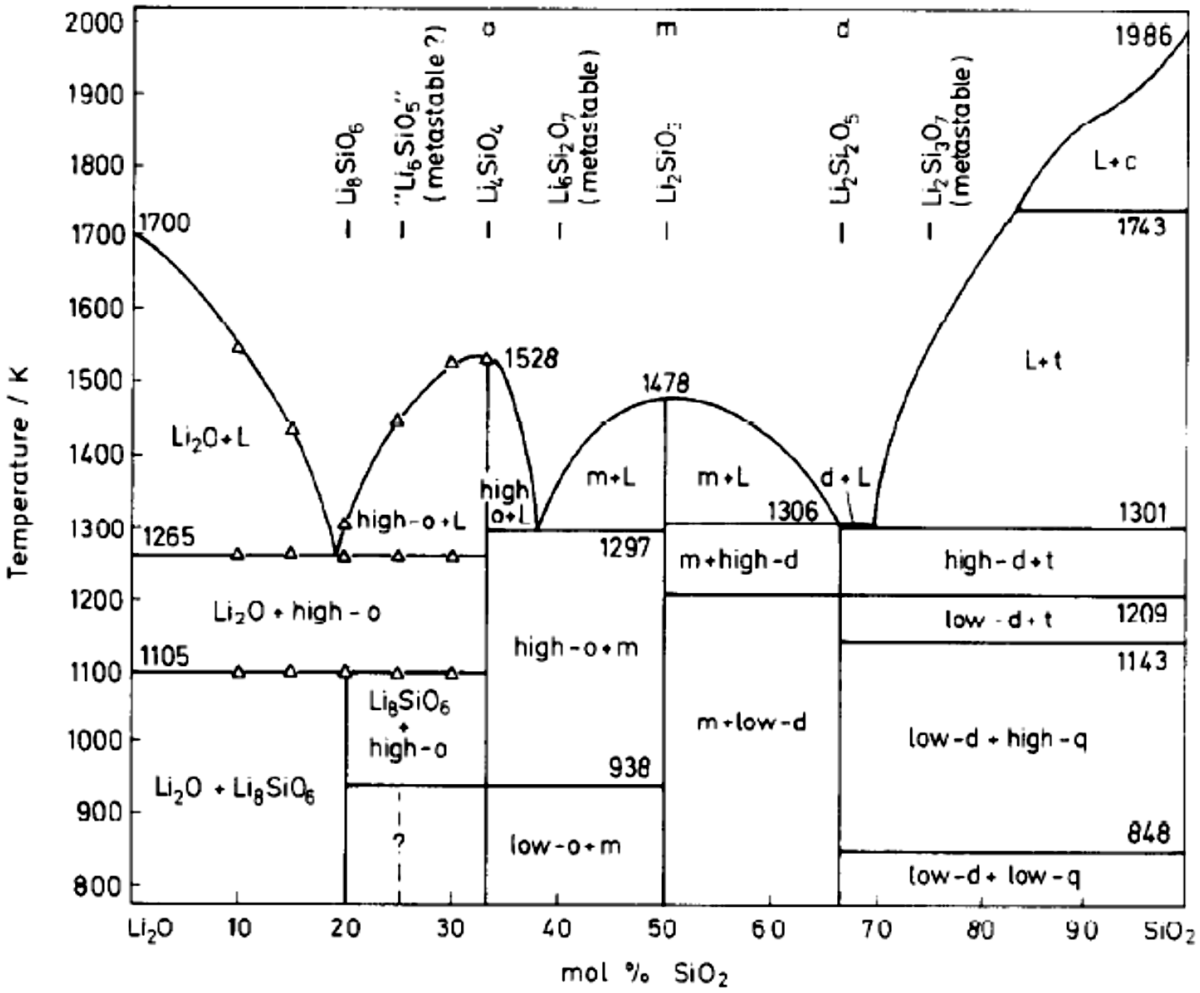

Fig.2.1The phase diagram of the Li_2O-SiO_2 system according to ref.[2]

Kracek et al[1] studied the equilibrium diagram of Li_2O-SiO_2 system. The intermediate position of Lithium between those of alkalis and the alkaline earths is evidenced in the nature of the compounds formed and in their properties. This transition character of lithium is very prominent in the compounds of silica. Alkalis have high basicity due to which they form stable compounds with high silica content. However, Orthosilicates of alkali metals are comparatively less stable than that of alkaline earth metals. Fig. 2.1 shows the equilibrium diagram of the Li_2O – SiO_2 system. From fig.2.1 it could be seen that the study is done with 0 – 100 mol% SiO_2.Three distinct phases of lithium silicates viz. Li_4SiO_4, Li_2SiO_3 and $Li_2Si_2O_5$

are seen for 33.3 mol%, 50 mol% and 66.67 mol% SiO_2 respectively. Below 20 mol% SiO_2 and above 1265K liquid phase of Li_2O is developed.

An important reaction occurs for the composition between 33.3 mol% SiO_2 and 50 mol% SiO_2 as temperature increases above 1273K. Li_4SiO_4 and Li_2SiO_3 forms eutectic point at 1297K. If the SiO_2 concentration is more or less than 33.3 mol%, it always produces a liquid phase. It is also seen that Li_4SiO_4 decomposes before its melting point is reached at 1528K and 33.3 mol % SiO_2.

2.2 Crystal Structure of Li_4SiO_4

Völlenkle et al[3] was the first to study the crystal structure of Li_4SiO_4. According to them, Li_4SiO_4had monoclinic structure with unit cell a =5.14Å, b = 6.10Å, c = 5.30Å and $\beta = 90.5^o$ and space group $P2_1/m$. The structure contains six different crystallographiacally Li atoms in which all lithium sites are partially filled with occupancy factors ranging from 1/3 to 2/3. However the structure proposed by him was not clear due to partial occupancy of lithium.

Dubey et al[4] stated that the crystal structure of Li_4SiO_4 was closely related to Li_4GeO_4 at ambient temperature with only difference in the position of lithium atoms in both cases. They determined the phase relations between Li_4SiO_4- Li_4GeO_4 and Li_4SiO_4- Li_4TiO_4 systems. At high temperatures (above 700^{o}C) all three phases Li_4SiO_4,Li_4GeO_4 and $Li_4TiO_4$are iso-structural. The lattice parameters values at low temperature (below 700^{o}C) were in agreement to that of *Völlenkle et al*. The low – high transition involved a change in the occupancy values of various lithium sites within the Li_4SiO_4.

Later,*Tranqui et al*[5] redefined the crystal structure of $Li_4SiO_4$by analyzing X-Ray diffraction data. They called the unit cell of Li_4SiO_4 as a 'superstructure' that contained 14 formula units, seven times larger than the earlier reported by *Völlenkle et al*. It also had monoclinic structure but the unit cell were a = 11.546 Å, b = 6.09Å, c = 16.645Å and β = 90.5^o and space group $P2_1/m$. The differences in the unit cell parameters may be due to the analysis of crystal structure of ordered Li_4SiO_4 by the authors which was not done by *Völlenkle et al*.

The unit cell of Li_4SiO_4 is shown below in fig.2.2

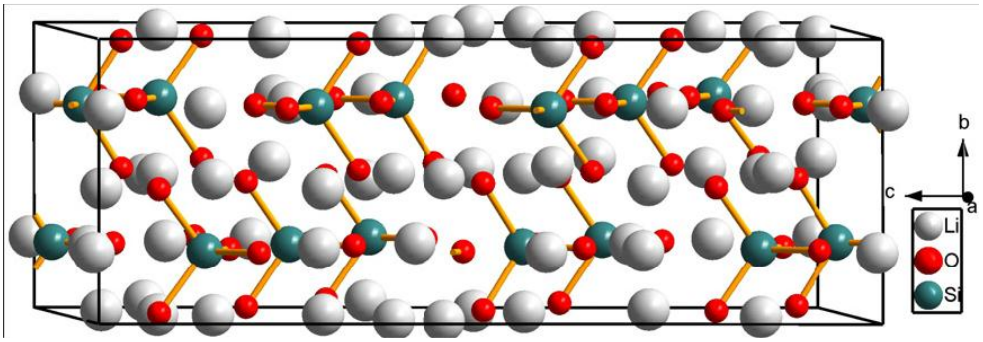

Fig.2.2 The crystal model (side view) of Li_4SiO_4'super structure'. The smallest, moderate and largest balls represent O, Li and Si atoms, respectively [8]

Munakata et al[6] examined the electron state of Li_4SiO_4 crystal by *ab-initio* calculation with CRYSTAL98 program [7]. According to the author the Li_4SiO_4contained isolated SiO_4tetrahedra with Li atoms floating around them. The crystal structure of Li_4SiO_4 contained 126 atoms (14 Si, 56 O and 56 Li) per unit cell. They located the positional parameters of each of 126 atoms in total present in Li_4SiO_4 crystal.

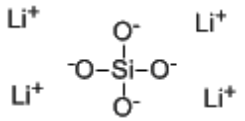

Fig.2.3 Schematic diagram of Li_4SiO_4

Tang et al[8] recently extended the work done by *Munakata et al* to understand the crystal structure, electronic structures, charge population of Li_2SiO_3 and Li_4SiO_4bulk and their mechanical properties. The author also used *ab – initio* calculation with Density Functional Theory (DFT) to calculate various atomic fractional co-ordinates of Li_4SiO_4. They found the Mulliken charges of Li ,Si and O atoms in Li_4SiO_4 with mean value of +0.59,+1.62 and -0.99 respectively. They directly calculated the Bulk modulus, Young's modulus and shear modulus values for Li_4SiO_4. Overall, the authors covered a broad area and gave a better understanding of Li_4SiO_4.

2.2 Synthesis of Li_4SiO_4

Use of different source of silica and different preparation method

Researcher used different processing technique like solid state mixing method, urea combustion method, water based sol-gel methodfor synthesis of Li_4SiO_4. Source of silica is important for synthesis of Li_4SiO_4. Generally, quartz powder, silicic acid, amorphous silica, fumed silica, TEOS are used as silica source. Quartz powder is cheaper but very much inert and not easily reacts with $LiOH/LiNO_3$.

Vollath et al[9],[10]deals with large scale production of $Li_4SiO_4$for which they have used amorphous silica. A suspension technique is used in which silica is suspended in methanol. After wetting ofsilica, LiOH is added. LiOH is dissolved while boiling at reflux. An insoluble organic intermediate is formed. Distillation of alcohol is done when a homogenous milky suspension is formed. The residue is then spray dried which is later calcined at 500^oC for 2-4 hr.Grinding yields the desired Li_4SiO_4powder. Only SEM micrographs of Li_4SiO_4powders were presented without any phase or thermal analysis. In other literature, *vollath et al*[11] synthesized Li_4SiO_4, along with Li_2SiO_3 and Li_6SiO_5 by spray-drying of the alcoholic suspensions followed by calcination of the residue and grinding as the final step. They studied the effect of various types of alcohol media in the synthesis of lithium silicates. They concluded that the presence of higher orders of alcohol produces more free carbon during calcination and that has to be removed by burning before using the powders.

Kaukis et al[12]prepared $Li_4SiO_4$by thermochemical methods using silicon dioxide and Li_2CO_3as the reactants. The homogenous mixture is grinded with anhydrous alcohol and dried at 390K. The dried mixture is calcined above 1125K which resulted in monophase Li_4SiO_4. However, no supporting data were given in relation with the phase purity.

Tao tang et al[13]prepared Li_4SiO_4through conventional solid state method by using amorphous silica and Li_2CO_3. Characterization techniques like TGA/DSC, XRD, SEM and BET surface area have been used. They studied the effect of Li/Si molar ratio (of 0.5, 1, 2and 4) and calcination temperature (700, 800 and 900^oC) on phase formation behavior. As for Li/Si = 4, 98% purity of Li_4SiO_4can be obtained at 700◦C. XRD result shows that phase pure Li_4SiO_4could be produced at 900^oC. SEM study shows that particle size is dependent on the synthesis temperature and Li/Si molar ratio. Large grains with side length 30μm and low

surface area (1.31m^2/gm) is formed. They explained the reaction mechanism and phase formation behavior by using TGA/DSC of the mixture of lithium carbonate and amorphous silica.

Cruz et al[14]utilized silicic acid as the source of silica for synthesizing Li_4SiO_4 along with Lithium hydroxide and Urea. They have varied the molar ratio of the reactants and heating temperature of furnace. The phase analysis has been done mainly by XRD and FTIR. It is found that highest percentage (~98%) of Li_4SiO_4along with minor quantities of Li_2CO_3 is obtained with 6:1:3 molar ratio of LiOH: H_2SiO_3: CH_4N_2O at 1100^oC with additional air in furnace during synthesizing. Presence of higher molar ratio of Li is detrimental as it favored the formation of Li_2CO_3.

Pfeifer et al[15]has used amorphous silica gel and TEOS as the source of silica. They have followed three different methods namely solid state, precipitation and sol-gel methods for the synthesis of Li_4SiO_4. Various characterization techniques used were XRD, TGA, SEM and BET for studying phase analysis and powder characterization. Pure $Li_4SiO_4$is formed by solid state method when calcined at 900^oC for 4 hrs. Non-homogenous polyhedral crystals with large particle size (~50µm) and low surface area (0.6m^2/gm) powders are obtained. Precipitation method and sol-gel method could hardly produce phase pure Li_4SiO_4. The powder prepared by above mentioned methods showed low surface area irrespective of the synthesis route followed.

Chang et al[16]utilized fumed silica with high specific surface area (~350m^2/gm) for the preparation of Li_4SiO_4. A solution based wet chemistry approach has been followed. Two different source of lithium has been used *viz* lithium nitrate and lithium hydroxide. The homogenously mixed solution of $LiNO_3$/LiOH and silica were then subjected to rotaryevaporationat a pressure of 600 mbar at 140$^oC$for 1 h, followed by a pressure of 100mbar at the sametemperature for 2 h.The Li_4SiO_4 phase begins to evolve at 500^oC when the as-prepared powders generated from LiOH.H_2O. In contrast, thepowders prepared from $LiNO_3$ show the formation of Li_4SiO_4 only after heat treatment at 600^oC. The difference in the formation temperature results from the different decomposition temperatures of both LiOH and $LiNO_3$.

Wu et al[17]utilized aerosil silica as the silica source for the synthesis of Li_4SiO_4along with hydrated LiOH. They followed water based sol-gel method in which citric acid is used as a chelating agent. First $LiOH.H_2O$ is dissolved in distilled water which is followed by the addition of citric acid. Later on aerosol silica is added to the clear solution and pH of the solution is maintained at 8.5. Phase pure Li_4SiO_4 is produced at 675^oC. Powder characterization techniques like BET surface area and SEM is done. This sol-gel derived powder has better sinterability over solid state derived powder.

2.3 Sintering and thermal stability of lithium orthosilicate compact

It is widely seen that sintering of lithium based ceramics is difficult due to low temperature (below 1000^oC) volatization of lithium from lithium compounds [18]- [20]. It is difficult to achieve more than 80% of the theoretical density [11], [17].

Wu et al[17] studied the sintering behavior ofLi_4SiO_4bar and found that linear shrinkage of about 5.2% occurred for the bar prepared from powders obtained by sol-gel method at 915^oC. Density of about 82.9 % RD was obtained at 1000^oC/4hrs. However no information was given on phase composition of the sintered product. Cruz et al [21] studied the kinetic analysis of the thermal stability of lithium silicates. According to their report Li_4SiO_4 decomposes to Li_2SiO_3 between 900^oC and 1000^oC. The decomposition was due to Li_2O sublimation. After the sublimation of Li_2O the tetrahedrons ofLi_4SiO_4 link among themselves to produce chain structures of Li_2SiO_3.

2.4 Moisture reactivity of Li_4SiO_4

The hygroscopic nature of lithium ceramic is a critical factor in the material selection for the design ceramics breeders, due to their moisture affinity. *Landeros et al*[22] studied the moisture reactivity of solid state derived Li_4SiO_4. They observed thatLi_4SiO_4 is able to trap water by two different mechanisms; adsorption and absorption. The characteristics of any of these sorption processes depend on different factors such as temperature and humid relative concentration. At higher temperature (more than 100^oC) and humid atmosphere produces different hydroxyls (Li-OH and Si-OH) instantaneously.

It is widely believed that the presence of water affects the tritium release behavior from ceramic breeders in the blanket. *Schauer et al*[23] did some isothermal adsorption and desorption of water on Li_4SiO_4powders. *Kawamura et al* [24] did some adsorption studies on Li_4SiO_4. According to him the adsorption of water was a dissociative phenomenon implying the decrease in the percentage of water capture with increase in temperature. *Hanada et al*[25] studied the effect of water on tritium release behavior in ITER Test blanket module. They found that presence of adsorbed water on the surface hinders the path of tritium movement. The Li_4SiO_4pebbles react with water and melts thereby covering the surface as shown in the SEM after the experiment.

2.5 Thermal properties of Li_4SiO_4

The design of Helium Cooled Pebble Bed (HCPB) blanket is affected by the thermal conductivity of the Lithium based ceramics (Li_4SiO_4 and Li_2TiO_3). A higher value of ceramic breeder pebble bed and bulk density of sintered samples (Pebble & pellets) is needed to improve tritium breeding ratio and thermal performance. In order to study the heat transfer in a blanket, the effective thermal conductivity of the pebble bed has to be known. *Lobbecke et al*[26] studied the effect of particle size and sample density on the thermal conductivity of Li_4SiO_4pebbles and pellets. The maximum value of thermal conductivity was 2.2 W/mK at 600^oC obtained for samples sintered at 1000^oC/2 hrs. *Dalle et al*[27] studied the effect of helium pressure variation on the effective thermal conductivity of the pebble bed. According to their reports pressure variation above 1 bar has no effect. The thermal conductivity value was found to decrease with temperature. The maximum value of effective thermal conductivity of the pebble bed with bed density of 65% was 1.2W/mK obtained at 800^oC. *Tanigawa et al*[28] measured thermal conductivity of Li_4SiO_4bed using silica coated hot wire method from room temperature to 700^oC. The maximum value of effective thermal conductivity was 0.95 W/mK at 700^oC. *Reimann et al*[29] measured thermal conductivity of $Li_4SiO_4$and Li_2TiO_3pebble beds. They calculated the effective thermal conductivity of the bed by pulsed hot wire method and compared with theoretically fitted SBZModel (Schlunder – Bauer - Zehner-Model [30]. The SBZ model has been frequently used to predictthe thermal conductivity, k, of pebble beds. This model takes into account the influences of parameterssuch as thermal conductivities of the pebble material, k_p, and gas, k_g, pebble

diameter d, bed porosityλ, and normalised contact area between pebbles. For Li_4SiO_4 pebbles with bed density of 64%, the effective thermal conductivity value decreased from about 3 to 2.25 W/mKwith increase in temperature from room temperature to 1000^oC.

Thus, it was found that the effective thermal conductivity was dependent on pebble material density and pebble bed density. The maximum value of thermal conductivity was found to be 2.2 at 600^oC.

2.6 Tritium release behavior of Li_4SiO_4

The primary function of a lithium containing ceramics is to breed tritium. The breeder must be maintained within a specified temperature range for acceptable tritium release. Lithium when irradiated with neutron produces tritium. The tritium is then recovered from the surface of the breeder material by a purge gas which contains hydrogen and helium, composition was mainly He+ 0.1% H_2 gas. Tritium generated in the breeder materials primarily by the reaction Li(n, 4He)T, is believed to diffuse across the grain to the grain boundary and then through the grain boundary to the network of interconnected pores and then surface reactions, desorption, and molecular diffusion in the gas phase i.e purge flow convection[31]-[33]. At the solid/gas interface between the effective bulk and the pores, tritium desorbs in molecular form as T_2, HT, T_2O and HTO depending on the chemistry of the solid and gas phase in the pores. Once tritium molecules desorb, they percolate through the network of fine pores to a purge stream which take out the tritium out of the breeder material[34]. The fact is that diffusion in the grain and desorption at the pore walls are two most rate-controlling mechanisms regarding tritium release. For better tritium release small grain microstructure and open pore structure is preferred.

2.7 Electrical properties of Li_4SiO_4

Electrical properties of breeder ceramics are of great importance not only concerning the appearance of electric and magnetic fields in fusion reactors during plasma operations but also regarding the tritium release. If the blanket zone forms a close circuit then the electric and changing magnetic field may cause electric current in the blanket material which leads to change in electrical properties of the sample. Electrical properties may also reflect some characteristic features of the microstructure[35]-[38]. The tritium ion is in the valence state of

$T^+$and is assumed to be bound with the oxygen ions. The migration of the tritium ions is assumed to occur by hopping from oxygen to oxygen ion in lattice. In such migration process the tritium must overcome the barrier of electrostatic repulsion due to lithium ions. Since the lithium ion is consider to migrate through vacancy mechanism, the lithium ion diffusion causes frequent replacement of lithium ion sites by lithium ion vacancy. Hence the repulsive force decreases and the tritium can easily migrate. So higher is the lithium ion conductivity higher will be the tritium diffusion. So, there is a quantitative similarity between lithium movement and tritium migration in solid breeder materials.

2.8 Other applications of Li_4SiO_4

Apart from Li_4SiO_4 being used as a promising material in tritium breeder applications in fusion reactors, it has got various other applications. Li_4SiO_4 has also been fabricated as ceramic membrane [39] and other forms [40], [41]for carbon dioxide absorbent. Li_4SiO_4 can absorb CO_2 upto $1/3^{rd}$ of its weight which is of special value for the fossil fuel industries. Substituting Si^{4+} by an aliovalent species like P^{4+} Li_4SiO_4 enhances the ionic conductivity to be used for high temperature battery applications [42]. Doping Co^{2+} in Li_4SiO_4 also makes it possible to be used as a cathode material in Li-Ion battery applications [43]. Lithium silicate is used as a stable solid electrolyte for thin film Lithium battery. The TFB (Thin Film Battery) with the Li_4SiO_4 electrolyte shows good reversibility [44].It is also used as a concrete hardener because it deeply penetrates and seals existing hardened floors.

References:

[1] F. C. Kracek, J. Phys. Chem. **34** {12} (1930) 2641.

[2] A. Skokan, H. Wedemeyer, D. Vollath and E. Gunther, in: Proc. 14th Symp. on Fusion Technology, Avignon, Sept. **8-12** (1986) 1255.

[3] H. Völlenkle, A. Wittmann, H. Nowotny, Die Kristallstruktur Von Li_4SiO_4, Monatsch .Chem. **99** (1968)1360.

[4] B. L. Dubey and A. R. West,J. InorgNucl Chem., **35** (1973) 3713.

[5] D. Tranqui, R. D. Shannon and H.-Y. Chen,ActaCryst. B**35**(1979) 2479.

[6] K.Munakata and Y. Yokoyama, J Nucl. Sci Tech.**38** [10] (2001) 915.

[7] V.R. Asuders, Crystal 98- User's manual

[8] T. Tang , P. Chen , W. Luoa, D. Luo , Y. Wang,J. Nucl. Mater. **420** (2012) 31.

[9] D. Vollath, H. Wedemeyer, E. Gunther and H. Elbel, Fusion Eng.Des.**8** (1989) 415.

[10] D. Vollath, H. Wedemeyer and E. Gunther,J.Nucl.Mater.,**133&134** (1985) 221.

[11] D. Vollath,H. Wedemeyer,J. Nucl. Mater.**141-143** (1986) 334.

[12] A.A. Kaukis, J.E. Tiliks, V.V. Tamuzhs, A.A. Abramenkovs, G.K. Kizane, J.A. Ubele V.G. Vasiljev, Fusion Eng. and Des. **17** (1991) 13.

[13] Tao Tang, Zhi Zhang, Jian-Bo Meng, De-Li Luo,Fusion Eng. Des. **84** (12) (2009) 2124.

[14] D. Cruz and S. Bulbulian, J. Am. Ceram. Soc.**88** [7](2005) 1720.

[15] H. Pfeifer, P. Bosch, S. Bulbulian,J. Nucl. Mater **257**(1998) 309.

[16] C.C. Chang, C.C. Wang, P.N. Kumta,Mater.Des.**22** (2001) 617.

[17] X. Wu, Z. Wen, X. Xu, X. Wang, J. Lin, J. Nucl. Mater.**392** (2009) 471.

[18] C.H. Lu, L.Wei-Cheng, J. Mater. Chem. **10** (2000) 1403.

[19] K. Essaki, K. Nakagawa, M. Kato, H. Uemoto, J. Chem. Eng. Jpn. **37** (2004) 772.

[20] H. Pfeiffer, K. M. Knowles,J. Eur. Ceram. Soc. **24** (2004) 2433.

[21] D. Cruz, S. Bulbulian, E. Lima, H. Pfeiffer,J. Solid State Chem. **179** (2006) 909.

[22] J. Ortiz-Landeros, L. M. Cruza, C. Gomez-Yanez, H. Pfeiffer,ThermochimicaActa**515** (2011) 73.

[23] V. Schauer and G. Schumacher,J. Nucl. Mater. **167** (1989) 225.

[24] Y. Kawamura, M. Nishikawa and K. Tanaka,J. Nucl. Mater. **208** (1994) 308.

[25] T. Hanada, S. Fukada, M. Nishikawa, K. Suematsu, N. Yamashita, T. Kanazawa,**85**(2010) 998.

[26] B. Löbbecke , R. Knitter, M. Rohde , J. Reimann, J. Nucl. Mater. **386–388** (2009) 1068.

[27] M. DalleDonne , A. Goraieb , G. Piazza, G. Sordon ,Fusion Eng. Des. **49–50** (2000) 513.

[28] H. Tanigawa, Y. Tanaka, M. Enoeda and M. Akiba,J. Nucl. Sci Tech, **46** {6} (2009)553.

[29] J. Reimann , S. Hermsmeyer,Fusion Eng. Des. **61-62** (2002) 345.

[30] E.V. Schlunder, Particle heat transfer, Proceeding of the 7th International Heat Transfer Conference, Munchen, Germany, 1RK10, (1982)195 .

[31] G.Federici, Wu C.H., A.R.Raffray and M.C.Billone, J.Nucl. Mater. **187** (1992) 1.

[32] T.Kinjyo, M.Nishikawa, M.Enoeda, S.Fukada, Fusion Eng. Des.**83** (2008) 580.

[33] A.R. Raffray, C. Seungyon, M.A. Abdou, J.Nucl. Mater. **210**(1994) 143.

[34] G.Federici, A.R.Raffray, M.C.Billone, C.H.Wu, S.Cho , M.A.Abdou, J.Nucl. Mater. **212-215** (1994) 1003.

[35] K.Noda, Y.Ishii,H.Matsui, H.Ohnoand H.Watanabe, Fusion Eng. Des.**8** (1989) 329.

[36] S.Konishi, H.Ohno, T.Hayashi, K.Okhunu, T.Matsuo, Adv Ceram **27**(1990)173.

[37] S.Konishi, H.Ohno, J. Nucl. Mater. **152** (1988) 9.

[38] K.Noda,Y. Ishii, H.Matsui, H.Ohno,S. Hirano and H.Watanabe, J. Nucl Mater.**155-157** (1988) 568.

[39] B.N. Nair , R.P. Burwood , V.J. Goh , K. Nakagawa , T. Yamaguchi, Progress in Materials Science **54** (2009) 511.

[40] M. Escobedo Bretado, V. Guzman Velderrain, D. Lardizabal Gutierrez, V. Collins-Martinez, A. Lopez Ortiz ,Catalysis Today **107–108** (2005) 863.

[41] C. Gauer, W. Heschel, J Mater Sci**41** (2006) 2405.

[42] A.D. Robertson, A.R. Westa, A.G. Ritchie, Solid State Ionics **104** (1997) 1.

[43] Z.L. Gong, Y.X. Li, Y. Yang,J. Power Sources **174** (2007) 524.

[44] A. Nakagawa, N. Kuwata, Y. Matsuda and J. Kawamura,J. Phys. Soc. Jpn. **79** (2010) Suppl. A, 98.

Chapter 3

Scope and Objective of Thesis

As discussed in the literature review, lithium orthosilicate (Li_4SiO_4) is one of the most promising solid breeder material in the tritium breeding blanket of thermonuclear fusion reactors, because of its higher lithium atom density than other lithium based ceramics, prominent tritium release rate at low temperatures between 200 and 400^oC, its low activation characteristics, low thermal expansion coefficient, high thermal conductivity. For tritium recovery purpose samples having 80-85% of true density with open porosity (around 10-12 %) is required. Uniform small grain size distribution (having diameter between 2-4μm) is preferable as activation energy for tritium diffusion through grain is higher compared to grain boundary. Solid state method requires higher calcination temperature, producing coarser particle and impurity, which adversely affects in achieving high sintered density (above 85% of theoretical density) and forms large grain size with entrapped closed pore inside the grain. The presence of closed pore affects the tritium release performance from ceramic breeders during neutron irradiation. Water adsorption properties of ceramic breeders are also an important aspect for the tritium release.

Most of the literature shows that the synthesis of Li_4SiO_4 powder is done using costly precursors of silica. In the present workLi_4SiO_4 powder was synthesized by solution combustion technique using cheaper precursor of silica i.e. from rice husk ash (an agricultural waste). Few reports are there regarding sintering of Li_4SiO_4 ceramic. Sublimation of Li_2O at high temperature (> 900^oC) possesses challenge to sinter Li_4SiO_4 ceramic to high density.

The present study aims to investigate the following points:

- Standardization of process parameters (e.g. metal to complextant ratio, calcination temperature) in solution combustion method by using cheaper source of silica from RHA to get phase pure powder at low temperature. For comparison Li_4SiO_4 will be also prepared by solid state route.
- To study phase stability at higher temperature (800^oC- 1100^oC) of synthesized powder and sintered ceramic.

- To achieve sintered density >80% of theoretical density at lower temperature (900^{o}C) and precaution will be taken to minimize the lithium loss from the sintered specimens.
- To study the kinetics of the initial stage of sintering from the shrinkage data to find out the sintering mechanism.
- To study pore size distribution of Li_4SiO_4 sintered ceramic using Mercury porosimetry technique.
- To study thermal conductivity of Li_4SiO_4 sintered ceramic by laser flash method.
- AC impedance method will be used to characterize electrical property of the sintered sample as tritium diffusion is related to the Li^+ ion conductivity in Li_4SiO_4.
- To study the moisture reactivity of sintered Li_4SiO_4.

Chapter 4

Experimental Work

4.1 Preparation of lithium orthosilicate powder

A solution combustion method has been utilized for the synthesis of Li_4SiO_4. Many researchers have attempted to use the heat generated by exothermic chemical reactions in the synthesis of various industrially useful ceramic materials. Various organic fuels like citric acid, urea, glycine etc. and nitrates of different metals have been used as the oxidant for the synthesis of various nanomaterials [1]-[6]. We have also tried to use the exothermicity during combustion to produce Li_4SiO_4. In this work we have synthesized Li_4SiO_4 by taking $LiNO_3$ as the starting Li source and amorphous silica as the Si source. Agricultural waste like Rice Husk Ash (RHA) has been taken as the source of amorphous silica. From the literature we found that many different source of silica (silicic acid, fumed silica, aerosol, quartz etc.) have been used for the synthesis of Li_4SiO_4. Silica from RHA has been selected as the source of silica because it was cheap, pure and easily available. The process of extraction of silica from RHA as well as different experimental techniques used for the study has been described below:

4.2 Preparation of amorphous silica precursor from RHA

Rice husk (RH) was collected from local rice mill. Unwanted fine dust materials and the physically adhered impurities were removed by washing properly with tap water. After successive washing, RH was dried in an air-circulated oven at 100 ± 2^oC for 12 h to get cleaned dried RH.

In the first purification treatment, cleaned husk was acid leached using 3 N HCl (Merck, India) solutions under boiling condition for 1 h followed by thorough washing with warm water to remove acid. In the second purification treatment, the leached husk was then dried and burned at 700^oC for 6 h in air atmosphere to get the rice husk whiskers. The rice husk whiskers were then pot milled for 6hrs using Iso-propyl alchohol (IPA) and 10 mm zirconia balls. After milling the solution (IPA + Rice husk ash) was dried overnight in an oven. The ash thus obtained was whitish in color and designated as WA. Fig. 4.1 shows the flow diagram of preparation of WA.

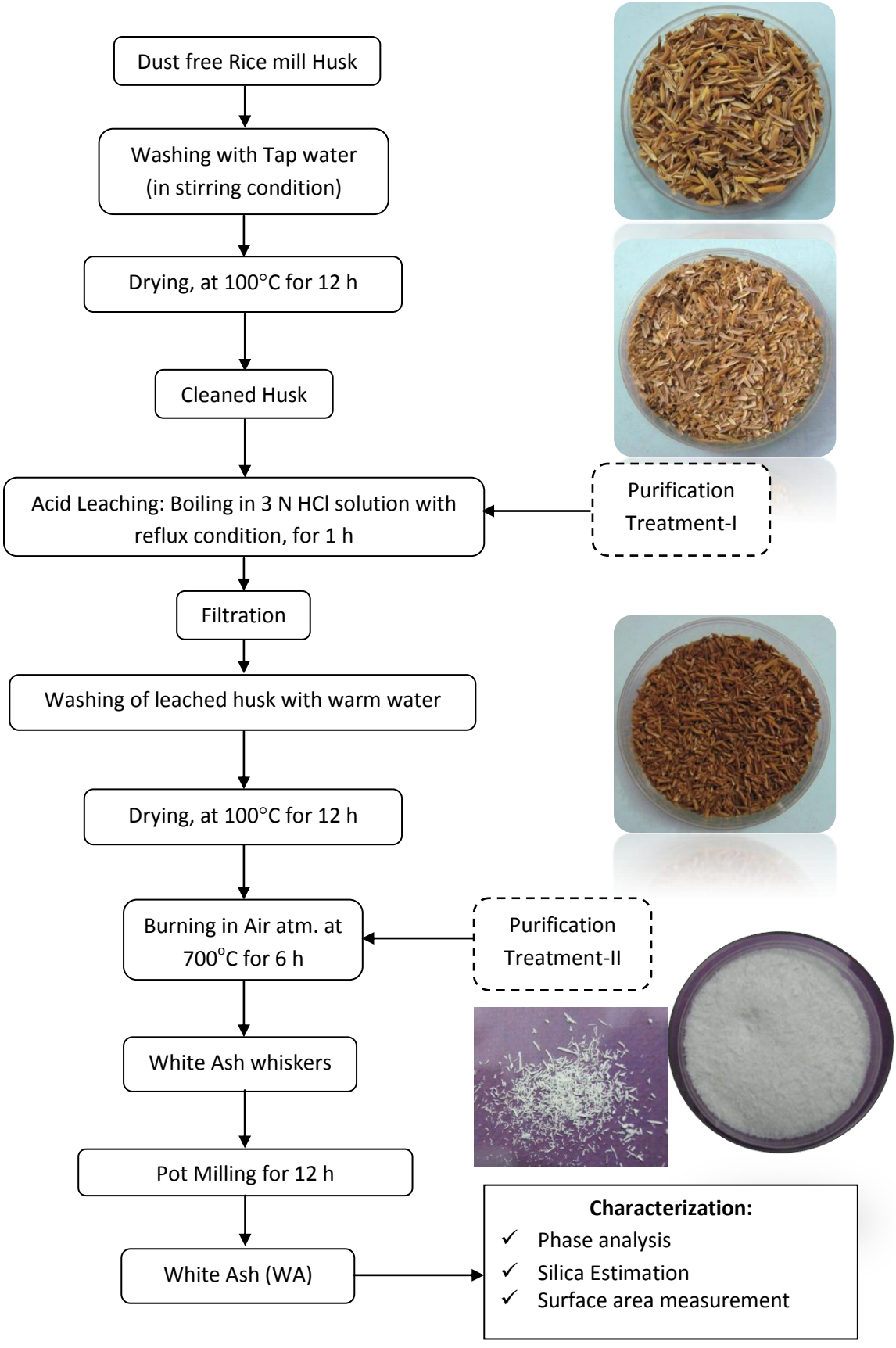

Fig 4.1: Flow chart for the preparation of silica from Rice Husk

4.2.1 Chemical analysis of Rice Husk Ash (RHA)

4.2.1.1Determination of LOI (Loss of Ignition)

Loss of Ignition (LOI) test was carried out to analyze the content of volatile organic compound inside the rice husk ash (RHA). The LOI of RHA was determined based on the SIRIM procedure (ISO 3262-1975). 1g of dried sample was placed in a platinum crucible and ignited in the muffled furnace at 1000^{o}C for 30 minutes to achieve constant mass, followed by cooling in a desiccator. The loss of ignition, as a percentage by mass, is given by the formula:

$$\% \text{ LOI} = [(m_o - m_1)/m_o] * 100 \qquad (4.1)$$

Where, m_o is the mass of the sample and m_1 is the mass of sample after ignition.

4.2.1.2 Determination of silica content

Silica content in RHA was measured based on the SIRIM method (ISO 3262-1975). 1 mL of 50% sulfuric acid had been slowly added into the residue obtained from LOI analysis. The crucible was heated gently until the fuming ceased and the heating was continued at 900^{o}C for 30 minutes in the muffled furnace, the residue was then removed from the furnace, cooled in the desiccator and weighed (m_2). The residue was dissolved in 1:5 mixture of H_2SO_4: HF solution, and evaporated on a hot plate until no further white fumes evolved. The crucible was ignited in the muffled furnace at 900^{o}C for 30 minutes, removed, cooled in the desiccator, and weighed (m_3). The silica content was calculated using following equation:

$$\% \text{ SiO}_2 = [(m_2 - m_3)/m_1] * 100 \qquad (4.\ 2)$$

4.3 Solution combustion synthesis of Li_4SiO_4

The starting precursors for the preparation of Li_4SiO_4 taken were Lithium Nitrate (Loba Chemie, 99%), amorphous silica from RHA and citric acid (CA, Merck, 99 %). Citric acid plays the role of fuel as well as complexing agent. Citric acid ($C_6H_8O_7$) has three carboxylic and one hydroxyl group for coordinating to metal ions and therefore prevents precipitation or phase segregation, thus providing an intimate blending among constituent ions. It is a low cost material and can be combusted with carbonates and nitrates (i.e. oxidant) at low ignition temperature (200–250^oC), and hence is a good choice as a fuel in the combustion technique. Another role of citric acid is it acts as complexing agent to the metal ions. We have varied the citrate to metal ratio, which was optimized to get uniform and complete combustion. Elemental stoichiometric coefficient (Φ_e) has been calculated to know whether the combustion reaction was fuel lean or fuel rich.

Φ_e is defined as

$$\phi_{\Phi e} = \frac{\sum(\boldsymbol{coefficients\ of\ oxidising\ elements\ in\ the\ spefic\ formula \times oxidising\ valence})}{(-)\sum(\boldsymbol{coefficients\ of\ reducing\ elements\ in\ the\ specific\ formula\ \times reducing\ valence})} = \boldsymbol{p/r}$$

where 'p' and *'r'* are integers representing the total composition of the oxidizing and the reducing elements respectively, in the mixture. A mixture is fuel rich if $\Phi_e < 1$, fuel lean if $\Phi_e > 1$, and stoichiometrically balanced at $\Phi_e = 1$. For calculatingΦ_e , the specific formulas of the oxidizer and the fuel components are first calculated. For different C/M values Φ_e was tabulated below:

Sl.No.	**C/M values**	**Φ_e**
1.	0.2	1.05
2.	0.45	0.744
3.	1.0	0.593
4.	1.2	0.56
5.	1.4	0.543
6.	1.6	0.53
7.	1.8	0.508

Table 4.1: Φ_e values for different C/M values

The valence of the element O has been taken as positive and those of elements Li, Si, C, and H as negative, with N taken as neutral [7].

The molar ratio of the citrate to metal ions was varied from 1.0 to 1.8 and the corresponding Φ_e values were from 0.593 to 0.508 respectively. In all the cases pH of the starting solution were at 1.

Stoichiometric amount of $LiNO_3$ and citric acid were mixed with required amount of water. A clear solution was obtained. Stoichiometric amount of Silica powder (White Ash from RHA) was added into the solution. The solution thus obtained was heated at 80-100^oC with constant stirring on hot plate. NH_4OH solution (Merck, 25%) was then added drop by drop under constant stirring in order to adjust the pH. The pH was maintained at 7 for all synthesis to have a neutral medium. The schematic flow chart of sample preparation was shown in Fig. 4.2. In all cases the combustion was slow and flameless. The as-burnt powder was calcined at 650°C for 6h to get better crystallization and finally ground to get Li_4SiO_4 breeder powder. For comparison samples of Li_4SiO_4 were also prepared by solid state reaction route. The stoichiometric amount of Li_2CO_3 (Qualigens, 98.5%) and SiO_2 (WA from RHA, 99.86 %) were taken and ball milled in iso propyl alcohol solvent. 15mm diameter Zirconia balls were used as grinding media.

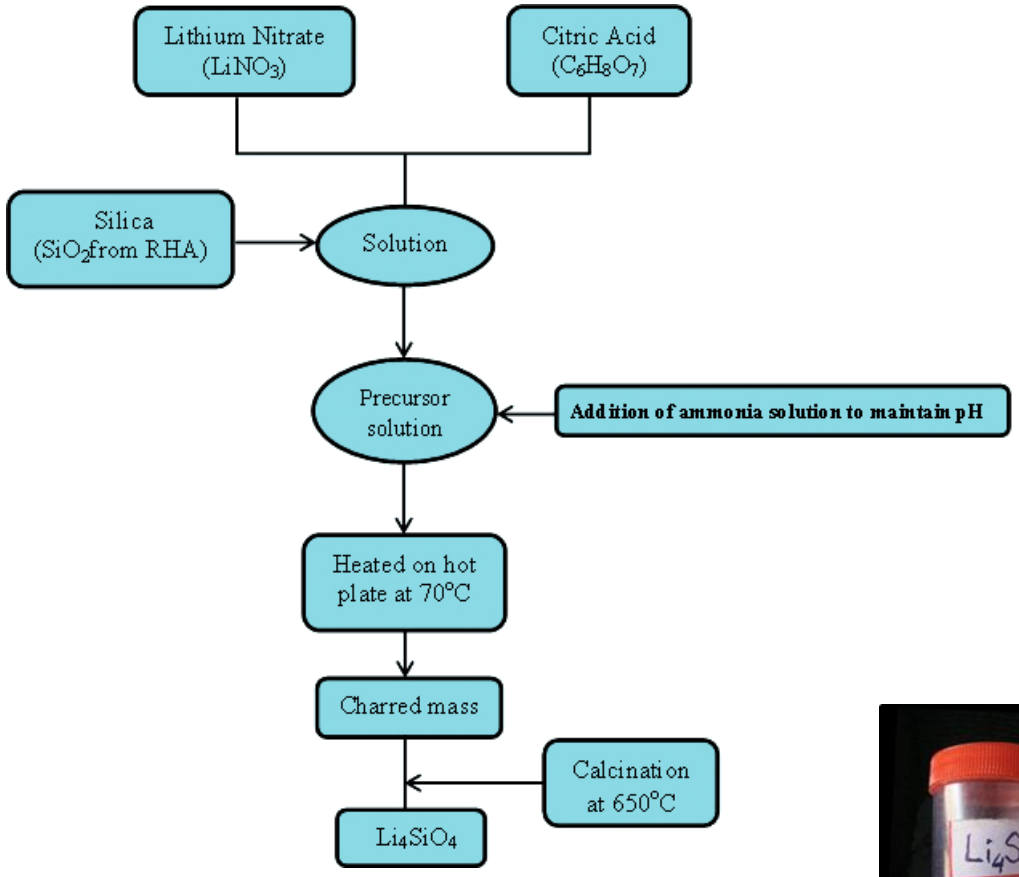

Fig. 4.1 Flow chart for preparation of Li_4SiO_4 using Solution – combustion method

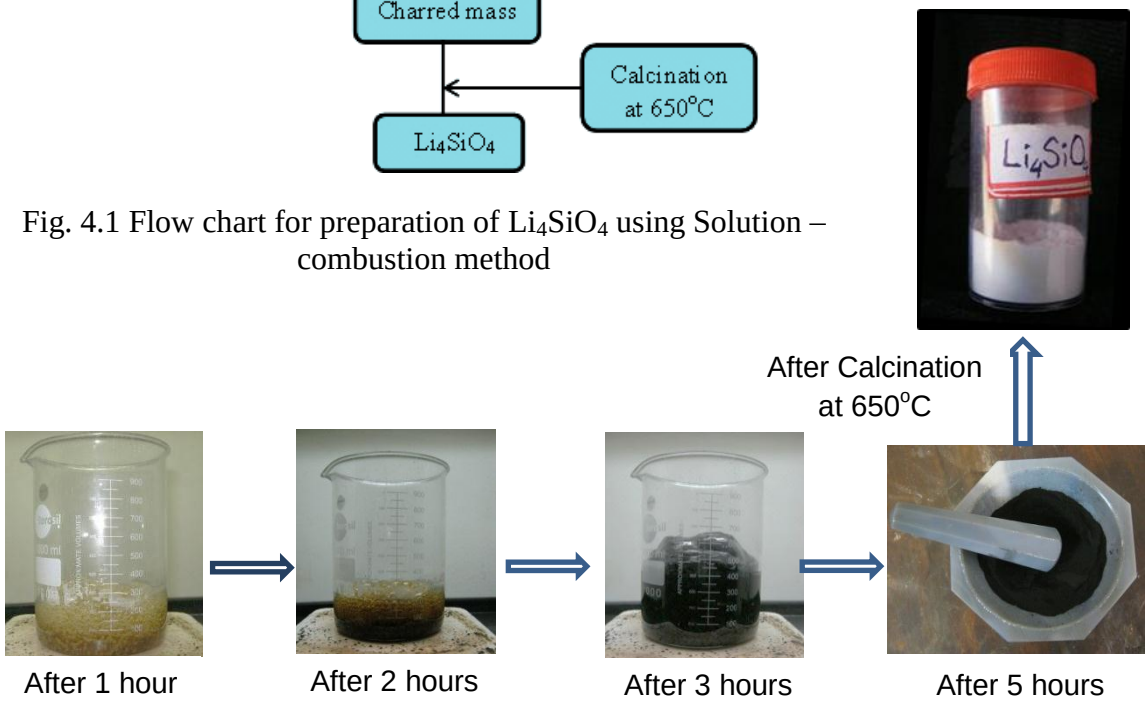

Fig. 4.3 Photographs of precursor soln. at different time elapsed during combustion

4.4 Characterization of dried gel and powder

4.4.1 Thermal analysis

The gel was collected prior the combustion and the dried gel was characterized by differential scanning calorimeter (DSC) and thermo gravimetric analysis (TGA) using NETZSCH STA (Model No 409C). DSC is the more recent technique and was developed for quantitative calorimetric measurements. The signal from the differential scanning calorimeter will be regarded as proportional to the difference in thermal power between the sample and reference, $d\Delta q/dt$. Differential scanning calorimeters make use of a crucible to contain the sample. The reference is either an inert material in a crucible of the same type as that used for the sample or simply the empty crucible. Crucibles commonly measure 5-6 mm in diameter made up of alumina. This technique is excellent for determining the chemical kinetics, enthalpy transitions and transformation, presence and quantity of hydrated water, decomposition behavior of gel, phase transitions, crystallization temperature and formation of products, etc. of precursor powders synthesized through different chemical route. Thermal analysis of dried gel has been carried out in air atmosphere with the heating rate of 10^{o}C/min from RT to 1000^{o}C. When a material undergoes physical or chemical change it absorbs or releases thermal energy. The temperature difference of the sample with respect to the reference inert material (α-Al2O3) during heating or cooling is plotted in a DSC curve as the deviation from zero base line. Exothermic or endothermic changes are shown in opposite directions of the baseline.

Theory of DSC:

The aim was to derive an expression for the instrument signal in response to the evolution of heat from a sample as represented by dh/dt. The sample and its crucible were considered as one with a total heat capacity C_P. A similar assumption was made regarding the reference material and its crucible, which together had a total heat capacity C_R. It was assumed that there was a source of thermal energy at temperature Tp and a single thermal impedance R between the sample and the source of thermal energy and between the reference and the source of thermal energy. The heat flow between the thermal energy source and the sample

was represented as dq/dt as measured by the instrument. The heating rate was represented by dT,/dt = p and assumed to be linear. Gray obtained the equation,

$$\mathbf{dh/dt = - dq/dt + (C_S - C_R)\, dT_P/dt - RC_S\, d^2q/dt^2}. \qquad (4.3)$$

Thus the heat evolution from the sample is given by the instrument signal measured from zero (term 1), a heat capacity displacement (term 2) and a third term which includes the product RC. This product has units of time so that (term 3) represents a thermal lag. Included in the publication was a recipe for obtaining dh/dt from the experimental curve by making allowance for thermal lag. For inert samples dh/dt = 0 and the displacement (term 2) provides a route to the determination of heat capacity.

Theory of TGA:

TGA is basically an analytical technique in which the mass change of a substance is measured as a function of temperature whilst the substance is subjected to a controlled temperature programme. The temperature programme must be taken to include holding the sample at a constant temperature other than ambient, when the mass change is measured against time. Mass loss is only seen if a process occurs where a volatile component is lost. There are, of course, reactions that may take place with no mass loss. As materials are heated, they lose weight due to drying, or from chemical reactions that liberate gasses. Some materials can gain weight by reacting with the atmosphere in the testing environment. The results may be reported directly as mass of the sample varying with temperature or time, i.e. as m versus T. Thus a mass loss appears as a downwards curve. Instead of mass in mg, the scale may be converted into percent of the original mass. An alternative is to convert the results into a percentage mass loss.

4.4.2 Crystallite size and phase analysis

Phase formation of as burnt and calcined powder samples were studied by the powder X-ray diffraction performed with a Philip's Diffractometer (model: PW-1830, Philips, Netherlands) using Cu Kα radiation. This technique gives some valuable information like crystal structure, crystalinity of the material, crystallite size, chemical analysis etc. The generator voltage and current was set at 35KV and 25mA respectively. The scan rate was 0.04^{o}/sec. the phases

present has been identified with the search match facility available with Philips X'pert high score software. A powdered sample was packed on a sample stage so that it can be scanned by the X-ray.

The diffracted X-rays were detected by an electronic detector placed on the other side of the sample. To get the diffracted beams the sample was rotated through different Bragg's angles. The goniometer keeps track of the angle (θ), and the detector records the detected X-rays in units of counts/sec and sends this information to the computer. After scan of the sample, the X-ray intensity (counts/sec) (Y axes) was plotted against the angle theta (2θ)(X-axes). The angle (2θ) for each diffraction peak was then converted to d-spacing, using the Bragg's law;

$$\mathbf{n\lambda = 2d\ Sin\theta} \tag{4.4}$$

where λ = wave length of x-ray

n = order of diffraction.

The crystallite sizes of the as burnt and calcined powder samples were determined from X-ray line broadening using the Schererr's equation [8] as follows:

$$t = {0.9\lambda}/{\beta cos\theta} \tag{4.5}$$

where, t is the crystallite size, λ is the wavelength of the radiation, θ is the Bragg's angle and β is the full width at half maximum. Line broadening due to instrument was subtracted from the peak width before calculating the crystallite size using the following formula:

$$\beta^2 = \beta^2_{obs} - \beta^2_{stan} \tag{4.6}$$

where, β_{obs} = measured full width at half maximum from peak, β_{stan}= instrumental broadening [Standard Silicon sample was used, whose β_{stan} value was 0.09821 at 2θ =29° with (hkl) value (111)].

4.4.3 Surface area measurement

Surface area of ceramic powder is an important parameter to predict sintering characteristics. This can be measured by BET (Brunauer, Emmet and Teller after the developers of the basic calculations) method. The BET method involves adsorbing a monolayer of nitrogen gas onto the surface of particles, then measuring the amount of nitrogen that is released when that

monolayer is vaporized. Based on this nitrogen quantity adsorbed, the surface area of the sample can be calculated from the BET equation:

$$\frac{1}{V_g}\frac{x}{1-x} = \frac{(c-1)}{cV_m}x + \frac{1}{cV_m} \tag{4.7}$$

where, V_g = volume of gas adsorbed, V_m = volume of gas adsorbed at monolayer coverage, x = P/P_o, P = Ambient pressure, P_o = Total pressure, c = a constant that is related to the heat of adsorption. A plot of $[(1/V_g)(x/(1-x))]$ versus x gives a straight line with slope = m = (c-1)/(cVm), Intercept = g = $1/cV_m$, The value of V_m and c are worked out, V_m = 1/(slope + intercept). This is normalized by the mass of particles tested to give a specific surface area (m^2/gm).

BET surface area of raw combustion powder as well calcined powder was measured using 5 point method by AUTOSORB 1, (Quantachrome) (Model No: Nova 1200 BET). The average particle size was estimated by assuming all the particles to have the same spherical shape and size. The average particle diameter, D (in nm), is given by:

$$D = \frac{6000}{S_p * \rho} \tag{4.8}$$

Where "S_{sp}" is the specific surface in m^2/g of the sample and "ρ" is the true density in g/cc.

4.4.4 Particle size analysis

A laser diffraction method with a multiple scattering technique has been used to determine the particle size distribution of the powder. Dispersed particles momentarily traversing a collimated light beam will cause Fraunhofer diffraction of light outside of the cross section of the beam when the particles are larger than the wavelength of the light. The intensity of the forward-diffracted light was proportional to the particle size squared, but the diffraction angle varies inversely with particle size. A He-Ne laser was commonly used for the light source. The combination of an optical filter, lens, and photo detector or a lens and multi element detector coupled with a computer enables computation of the particle size distribution from the diffraction data. The sample may be either a liquid or gas suspension of particles or droplets of about 0.1 vol % concentration. It was based on Mie-scattering theory.

In order to find out the particles size distribution the Li_4SiO_4 powder was dispersed in water by horn type ultrasonic processor [Ultrasonic Processor Sonopros, PR1000 MP].Then experiment was carried out in computer controlled particle size analyzer [ZETA Sizers Nanoseries (Malvern Instruments Nano ZS)] to find out the particles size distribution.

4.5 Compaction behaviour of powder

The packing characteristic of particles, stress induced flow behaviour and the agglomeration strength of calcined powder were studied from the logarithmic pressure- relative density diagram. Compaction behaviour and agglomerate strength of the powder has been measured by uniaxially compaction of the powder in circular die and punch. The weighed amount of powder was taken in a stearic acid lubricated die and punch. The powder was properly leveled and the initial height was of the powder was measured. The punch movement was measured using universal testing machine (UTM) (Hounsfield H50KT, UK) at a constant crosshead speed of 0.2 mm/min. The green density of the powder compact has been calculated from the punch movement and the initial height of the powder.

4.6 Preparation of bulk sample

Calcined powder was mixed with 1-3 wt. % PVA (Poly Vinyl Alcohol) binder with the help of mortar and pestle. The binder mixed powder was compacted to give a desired shape for further characterization. The binder mixed powder was dried and granulated. The granules were uniaxially pressed using a hydraulic press at a pressure of 275 MPa for 2 minutes (4T, Carver Inc ,USA) to form cylindrical pellets (Dia-12.5 mm, thickness-2 mm). Some samples were pressed for thermal conductivity measurement having diameter 15mm and height 3mm in a cylindrical die of dimension 15mm diameter and 500mm height. Green densities were calculated from weight/volume ratio. Weight was measured using electronic balance whereas; volume was calculated from the dimension of the specimens.

4.7 Densification study of powder compact

Shrinkage behavior of the green compact and thermal expansion of sintered bar shaped samples were investigated by NETZSCH dilatometer model DIL 402 C. In the dilatometer the specimen was kept in a specimen holder in the centre of the furnace. The linear dimensional change i.e. shrinkage or expansion of the specimen was transmitted through the push rod (pressed against the sample inside the furnace) to the measuring head.

Samples size was bar having diameter 6 mm and length 15 mm for dilatometer experiment. The heating rate was maintained at 10^{o}C/min. The measurement was carried out from room temperature to 900^{o}C in air atmosphere.

4.7.1 Sintering kinetics

The sintering kinetics Li_4SiO_4 powder was studied by non-isothermally constant rate heating method. In the constant rate heating method, the green rectangular bars of Li_4SiO_4 was sintered at different heating rate (3,5 and 10°C/min) till 900°C in ambient atmosphere in a dilatometer (NETZSCH DL 402C).The activation energy for mass transport during initial stage of sintering was calculated from the shrinkage data at different temperatures. An attempt was made to sinter Li_4SiO_4 samples by using different heating rate and soaking period at predetermined sintering temperature.

4.7.2 Sintering study

Sintering of green compacts was carried out `in a chamber furnace (45R5Y) by heating it from room temperature to 650^{o}C at a heating rate of 3^{o}C/minute with a holding time of 30 minute at 650^{o}C for binder removal. Thereafter, the heating was continued at the rate of 2^{o}C/minute till the final sintering temperature was attained. A holding time was provided at the peak sintering temperature. Following the sintering, the samples were furnace cooled to room temperature.

4.7.3 Sintering methods utilized

In order to increase the density of the Li_4SiO_4 sample and to minimize Li_2O sublimation, following sintering arrangement has been used during sintering.

Sintering method-I

In Sintering method-1, 2 gm of Li_2CO_3 were fired in an alumina crucible covered with lid at 700^oC for 2 hrs. Later on the same crucible was used for sintering of Li_4SiO_4 pellets with a bed of remaining Li_2CO_3. The diagram for the sintering arrangement was shown below:

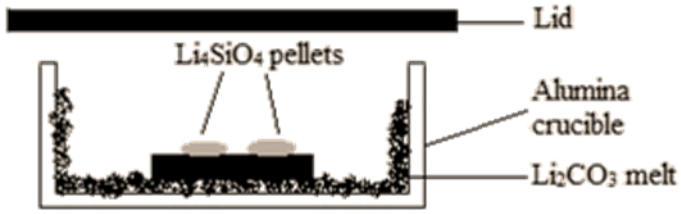

Fig 4.4 Arrangement of sintering method-1

Sintering method-II

In sintering method-II, 2 gm of Li_4SiO_4 were fired in an alumina crucible covered with lid at 700^oC for 2 hrs. Later on pellets were kept on a bed of Li_4SiO_4 powder and they were covered with the same Li_4SiO_4 powder. The diagram for the sintering arrangement was shown below:

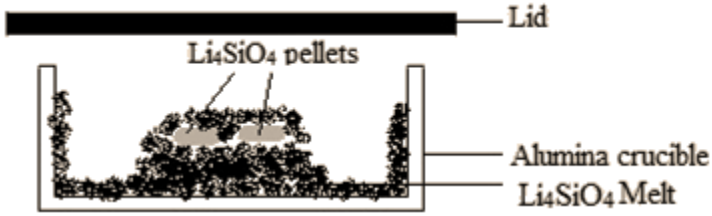

Fig.4.5 Arrangement of sintering method-II

Sintering method-III

In sintering method-III, 10%/20%/30% excess Li batches of Li_4SiO_4 were prepared and later on Li_4SiO_4 was sintered on the bed of these excess Li batches. The diagram for the sintering arrangement was shown below:

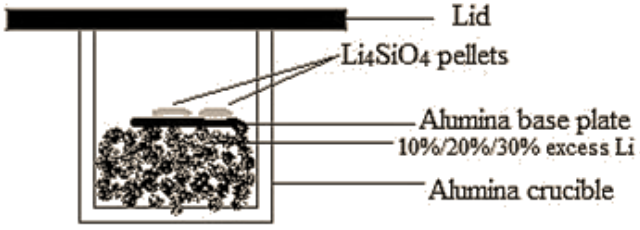

Fig4.6 Arrangement sintering method-III

4.8 Density and apparent porosity

Bulk density and apparent porosity of sinter specimens were determined by Archimedes principle. Sintered samples were weighted in dry state. Samples were immersed in kerosene and kept under a vacuum desiccators 4 hrs to ensure that kerosene filled up the open pores completely. Then, soaked and suspended weights were measured. The apparent porosity and bulk density were calculated as follows:

W_d =Dry weight of the sample,

W_s = Soaked weight of the sample,

W_a =Suspended weight of the sample

$$\text{Bulk density} = \frac{W_d}{W_s - W_a} \text{ X Density of kerosene} \quad (4.9)$$

$$\text{Apparent porosity} = \frac{W_s - W_d}{W_s - W_a} \text{ x } 100 \quad (4.10)$$

4.9 Mercury porosimetry

For tritium release we require about 10-15% porosity in lithium based ceramics. The amount of porosity and the pore size distributions in Li_4SiO_4 were measured by Hg Porosimetry Analyzer, Poremaster, PR-33-13 (Quanta chrome Instruments, Germany). The technique is based on the phenomena of capillary rise as shown in fig.4.7 Sintered sample were fractured by using pliers and the sample holder was filled with 1-2 such broken pieces.

Mercury does not wet most ceramic materials, and pressure must be applied to force it into evacuated surface pore. A typical mercury intrusion porosimetry test involves placing a sample into a container, evacuating the container to remove contaminant gases and vapors (usually water) and, while still evacuated, allowing mercury to fill the container. This creates an environment consisting of a solid, a non-wetting liquid (mercury), and mercury vapor. Next, pressure is increased toward ambient while the volume of mercury entering larger openings in the sample bulk is monitored. When pressure has returned to ambient, pores of diameters down to about 12 mm have been filled. The sample container is then placed in a pressure vessel for the remainder of the test. The maximum pressure range is about 33 Kpsia

which will force mercury into pores down to about 0.003 mm in diameter. The volume of mercury that intrudes into the sample due to an increase in pressure from Pi to Pi+1 is equal to the volume of the pores in the associated size range ri to ri+1, sizes being determined by substituting pressure values into Washburn's equation.

$$R = \frac{-2\gamma_{LV}\cos\theta}{P} \tag{4.11}$$

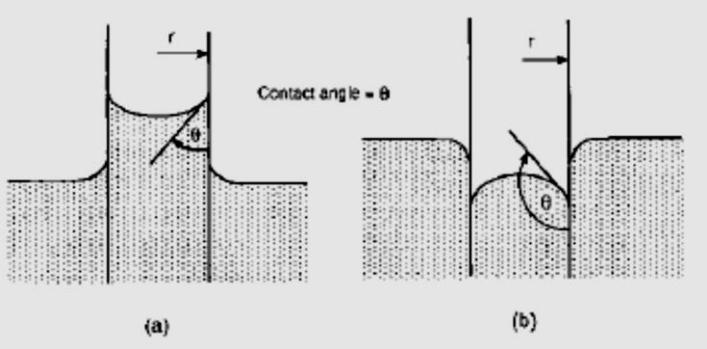

Fig4.7 Capillary rise phenomena for (a) Wetting liquid(contact angle <90^o)
(b) ANon-wetting liquid (contact angle >90^o)

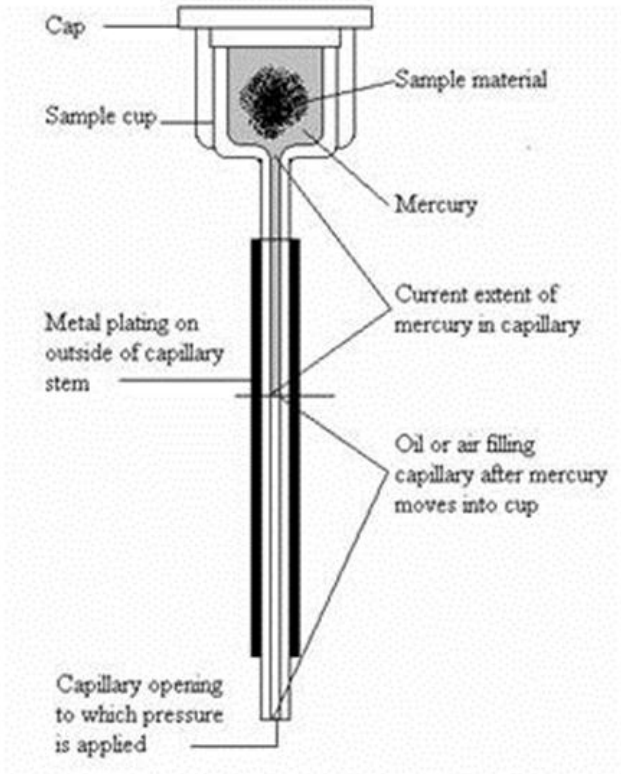

Fig 4.8: Cross-section of a penetrometer in which pressure has forced some mercury into the pores of the sample and about 50% of the stem capacity has been used.

4.10 Moisture reactivity of Li_4SiO_4

The absorption of moisture plays a critical role in lithium based ceramics. Sintered samples were kept in a SECADOR dessicator cabinet with air tight facility for two different duration of time i.e 1 day and 1 week. A uniform relative humidity of about 94.6% was maintained using boiled and normal DI water. For comparison purpose 1 sintered sample was also kept in Vaccuum oven (IndVac systems) at 110^{o}C for 24 hrs. Later on these sintered samples were crushed into powders for FTIR analysis.

4.10.1 Fourier Transformed Infrared (FTIR) analysis

FTIR spectroscopy was used to characterize the chemical functional groups present in materials, based on the characteristics of vibrational and rotational energies of different molecular bonds. FTIR analyses of raw, calcined and sintered powder (kept at different durations with a constant humidity condition) were done at a resolution of 4 cm-1 using Spectrum RX-1 instrument (Perkin Elmer) in the wave number range 400 to 4000 cm-1 using the KBr wafer technique. The sample was mixed with KBr in the ratio of 1mg sample to 300 mg KBr. The mixture was ground to a finely divided powder in an agate mortar and a disc was prepared under 10 tons of pressure for 1 minute to obtain self – supporting pellet. The spectrogram of the sample is observed on computer monitor and a graphic representation of the spectra was taken.

4.11 Microstructural analysis

Microstructural analysis is one of the important interpretation tool regarding the tritium release property of breeder material. For tritium recovery purpose we need samples having 85-90% of TD with a significant open porosity of 5%. Again Uniform grain size distribution having diameter between 2-4μm is required for this purpose.

In the SEM, a source of electrons is focused (in vacuum) into a fine probe that is rastered over the surface of the specimen. As the electrons penetrate the surface, a number of interactions occur that can result in the emission of electrons or photons from (or through) the surface. A reasonable fraction of the electrons emitted can be collected by appropriate detectors, and the output can be used to modulate the brightness of a cathode ray tube (CRT)

whose x- and y inputs are driven in synchronism with the x-y voltages rastering the electron beam. In this way an image is produced on the CRT; every point that the beam strikes on the sample is mapped directly onto a corresponding point on the screen.

As fired samples and the fractured surface were cleaned in acetone and dried at 100^{o}C for 24hr for SEM imaging. Some sample surfaces were polished on fine emery paper; the samples were thermally etched at 50^{o}C less than the sintering temperature. Powder samples were dispersed in water medium in ultrasonic vibrator (Oscar, Sonopros PR-1000MP). One drop was put on a glass plate and dried under IR lamp for 4 hr prior to the SEM imaging.

4.12 Electrical conductivity measurements

For electrical characterization the sintered pellets were polished by fine emery paper to make their faces smooth and parallel. Samples were painted by conducting silver paste on the parallel surfaces followed by curing at 500^{o}C for 30 minutes. The AC resistivity (ρ) was calculated using the formula

$$\rho = RL/A \tag{4.12}$$

Where R= Resistivity

L= Thickness of sample

A=Area of cross section

The conductivity was calculated by taking the inverse of ρ

At low fields, this means at average applied fields F (i.e., the applied voltage V divided by the specimen thickness d) lower than the threshold (or critical) field F_{th} for switching on significant injection of carriers from the carrier injecting contacts. Electrical conductivity follows the empirical equation given by

$$\sigma = \sigma_o \exp(-Ea/kT) \tag{4.13}$$

Where σ_o is the pre exponential factor and Ea is the activation energy, k is Boltzmann's constant and T is temperature in Kelvin.

4.13 Thermal Conductivity measurement

Several techniques are used to measure thermal conductivity (k_{th}) in solids. One method that has gained popularity recently is the laser flash technique. This technique attempts to measure the time evolution of the temperature on one side of the sample as the other side is very rapidly heated by a laser pulse. As it passes through the solid, the signal will be altered in two ways: There will be a time lag between the time at which the solid was pulsed and the maximum in the response. This time lag is directly proportional to the thermal diffusivity (α), of the material. The second effect will be a reduction in the temperature spike, which is directly related to the heat capacity (c_p) of the solid. The heat capacity, thermal diffusivity , and thermal conductivity and density are related by:

$$K_{th} = \rho C p \alpha \qquad (4.14)$$

The conduction of heat through solids occurs as a result of temperature gradients. Thermal energy in solids is transported by lattice vibrations, i.e. phonons, free electrons, and radiation. In ceramics the concentration of free electrons is very less thus the phonon mechanism virtually responsible for the thermal conduction. When a solid is heated, the atoms in that region will have large amplitudes of vibration and will vibrate violently around their average positions. This sets the neighboring atoms into oscillation. As a result the disturbance, caused by the application of heat, propagates outward in a wavelike manner. These waves, in complete analogy to electromagnetic waves, can be scattered by imperfections, grain boundaries and pores or even reflected at other internal surfaces. So, thermal conductivity depends upon several parameters which can be controlled by adopting new processing steps.

References

[1] X. Zhai, Y. Fu, G. Chu, Nanoscience **11**{4} (2006) 286.

[2] T. Singanahally Aruna , S. Alexander Mukasyan, Current Opinion in Solid State and Mater. Sci. **12** (2008) 44.

[3] V.B. Bhatkar , S.K. Omanwar , S.V. Moharil, Optical Mater. **29** (2007) 1066.

[4] R.D. Purohit , S. Saha , A.K. Tyagi, J. Nucl Mater **288** (2001) 7.

[5] T.Mimani and K.C.Patil, Mater. Phys.Mech. **4** (2001) 134.

[6] R.S. Guo , Q.T. Wei, H.L. Li, F.H. Wang, Mater. Lett. **60** (2006) 261.

[7] M. Barrere, A. Jaumotte, B.F. DeVeubeke, J. Vandenkerekhove, Rocket Propulsion, Elsevier, Amsterdam (1960) 132

[8] B. D.Cullity,Elements of X-Ray Diffraction‟, 2nd Ed, Addision-Wesley. INC (1978).

Chapter 5

Results and Discussions

5.1 Optimization of process parameters for the synthesis of Li_4SiO_4

Solution combustion synthesis (SCS) is a versatile, simple and rapid process, which allows effective synthesis of a variety of nanosize materials. The synthesis of lithium orthosilicate by solution based combustion technique requires optimization of process parameters (like fuel to oxidizer ratio, pH and metal to citrate ratio).Optimizations of metal to citrate ratio and calcination temperature on the formation of Li_4SiO_4 powder have been discussed below:

5.1.1 Optimization of citric acid to metal ratio

The metal to citric acid ratio (C/M) was varied from 1.0 to 1.8 at the interval of 0.2. Citric acid behaves as a metal complexant as well as fuel for the combustion. It was found that for C/M<1.4, phase pure Li_4SiO_4 could not be produced. The nature of combustion was slow for all C/M values. To have a better understanding of the combustion process, elemental stoichiometric coefficient Φ_e [1] was calculated (details are given in Experimental work, chapter-4, page no.31) for each experimental C/M ratios. It is known that if the value of Φ_e is less than 1, indicates that the composition is fuel rich. It was found that phase pure Li_4SiO_4 was produced for the values of C/M $\geq$ 1.4; those are also fuel rich composition. Thus, Φ_e values confirm the slowness of the reaction. Only for C/M = 0.2, we get Φ_e = 1.05 which indicates a fuel lean condition. But, at that citric acid content amorphous silica was not dissolved in the solution so it is discarded.

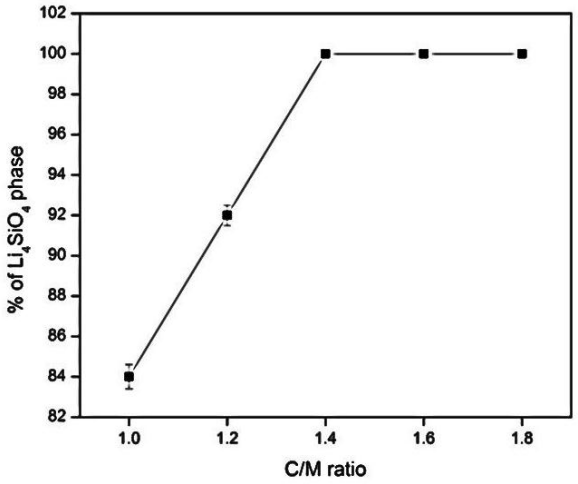

Fig.5.1: Effect of C/M ratio on Li_4SiO_4 phase formation

Fig 5.1 show the effect of variation of C/M ratio (1.0-1.8) on the percentage of Li_4SiO_4 phase formed in the calcined powder. For lower value of C/M ratio (1.0 and 1.2) 84% and 92% Li_4SiO_4 respectively were obtained. For C/M values ≥ 1.4, 100% Li_4SiO_4phase could be observed. To determine the weight percentage, p, of the compounds detected by XRD, it was assumed that the most intense diffraction peak of each compound was proportional to the percentage in the sample, and it was calculated by Eq. (5.1):

$$p = \frac{C_i}{\sum_j C} 100 \qquad (5.1)$$

Where C_i represents the integral intensity corresponding to each compound identified, and $\Sigma_j C$ is the addition of the integral intensity corresponding to all the compounds identified in the sample[2].

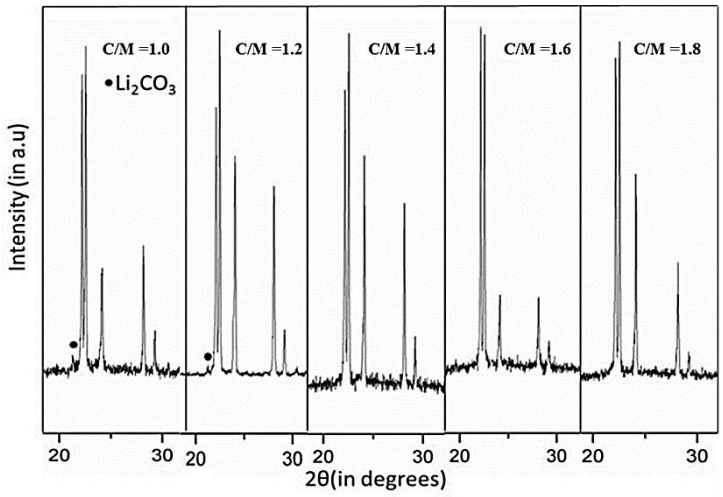

Fig.5.2: XRD at C/M ratio 1.0 to 1.8 for $17.5^o<2\theta<32.5^o$

Fig. 5.2 shows the XRD patterns for C/M=1-1.8.In order to highlight some of the impurity phases, the pattern from $2\theta 17.5^o$ to 32.5^o has been shown in the above figure. The as-burnt powders were collected and fired at 750^oC to analyze the phase formation of Li_4SiO_4. Beyond a certain C/M ratio (1.4) phase purity is independent of C/M ratio (Fig.5.1). Here citric acid has dual role it acts as a complexant for metal ions and fuel for combustion reaction. The requirement for higher C/M ratio may be due to at low citric acid content chelation was poor andsome metal ions like silicate remains free in the solution.The peak of

lithium carbonate was shown for C/M ratio less than 1.4 and that may have remained due to improper chelation.

5.1.2 Optimization of calcination temperature

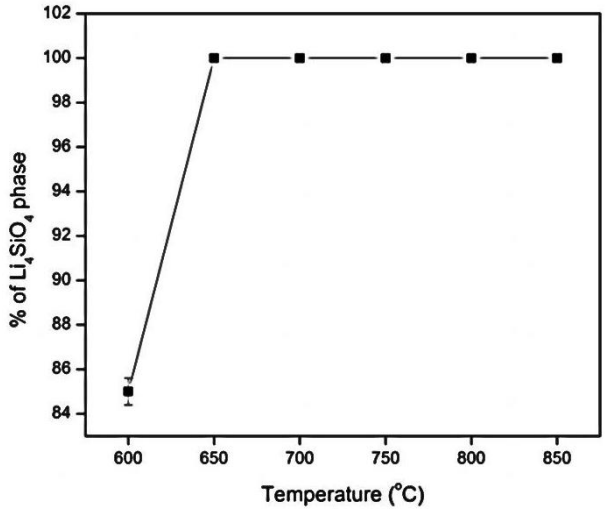

Fig.5.3: Effect of calcination temperature on Li_4SiO_4 phase formation

After optimizing the C/M ratio for the solution combustion route (SCR), the calcination temperature was optimized for getting phase purity in the calcined product. The as-burnt raw powders were calcined at temperature ranging from 600 to 850^oC; at an interval of 50^oC. Fig.5.3 shows the variation of calcination temperature with the weight percentage of Li_4SiO_4phase formation. It was seen that at 600^oC, only 85% Li_4SiO_4 phase was obtained with 15% of other impurity phase. The percentages of different phases were found by using eqn.5.1. XRD at different calcination temperature ranging from 600 to 750^oC was shown in fig.5.5. It was clear that phase pure Li_4SiO_4could be produced for the calcination temperature more than 650^oC.

5.2 Thermal and phase analyses of SCR derived Li_4SiO_4 powder

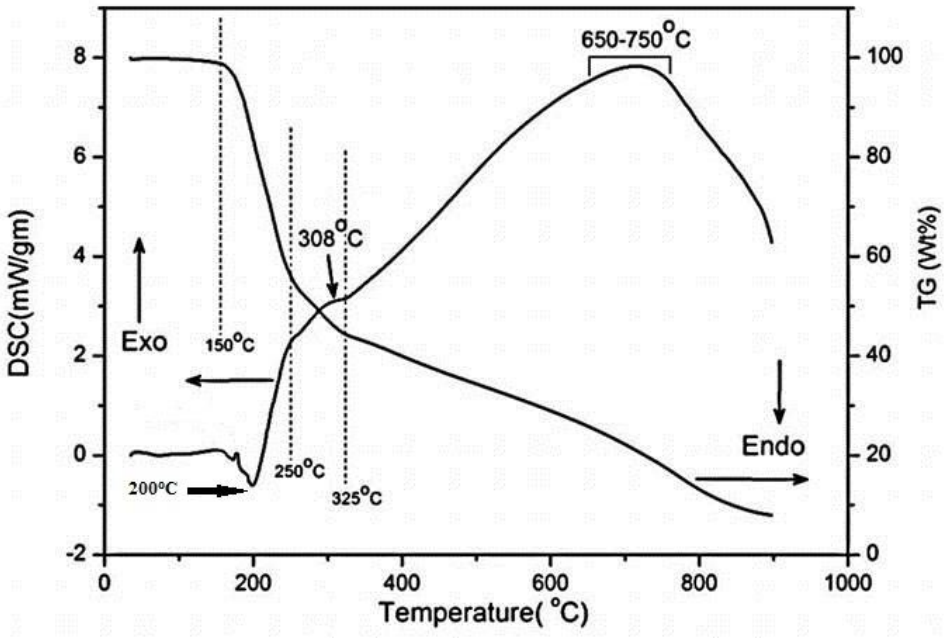

Fig.5.4: DSC-TG Plots of the gels with C/M =1.4 (SCR samples)

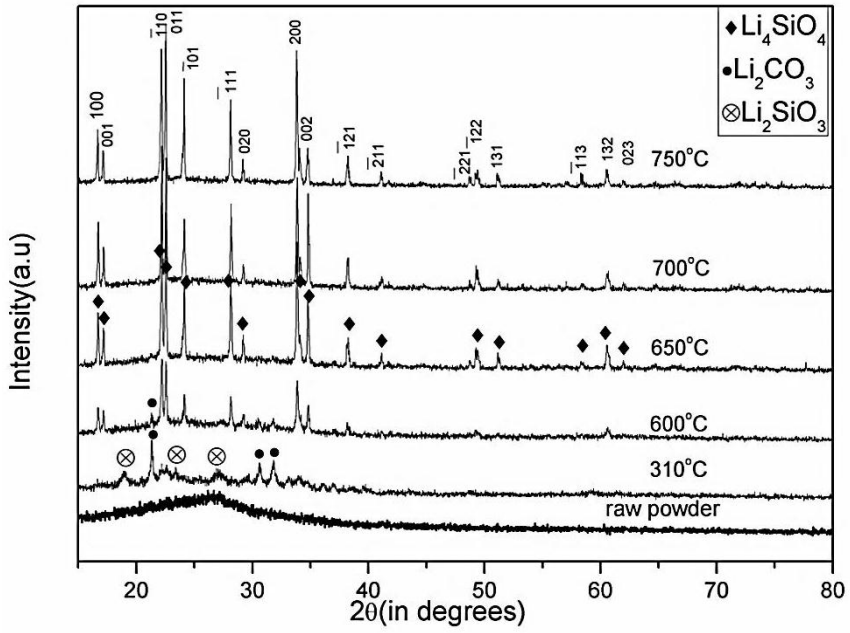

Fig. 5.5: XRD pattern of Li_4SiO_4 powder with C/M=1.4 (SCR samples)

Fig.5.4 shows the DSC/TG plots of the gel samples (collected prior to combustion) with C/M =1.4 (SCR sample). An overall weight loss of around 90% was observed in as prepared SCR gel samples from the TG curve.An endothermic peak was found in DSC curve at around 200^{o}C, which was probably due to the decomposition of metal-citrate complex [3].Simultaneous weight loss of ~45% was observed in the corresponding TG curve in the temperature range 150-250^{o}C. Further, a weak exothermic peak was found in DSC at 308^{o}C, which was associated with the carbonization of gel and simultaneous formation of Li_2CO_3 and Li_2SiO_3[4] as confirmed from XRD patterns (shown in fig.5.5) of powder calcined at 310^{o}C. The homogenous mixing in the solution phase and presence of citric acid may have favored the formation of Li_2SiO_3 at a lower temperature compared to SSR. The broad exothermic peak also indicates that there was continuous heat evolved above 325^{o}C until 750^{o}C which indicated that formation of $Li_4SiO_4$and burning of the carbonaceous matter might have taken place over a range of temperature rather than a particular temperature.The formation of Li_4SiO_4 was via the reaction of $Li_2SiO_3$with Li_2CO_3as given by eqn. $Li_2CO_3 + Li_2SiO_3 \rightarrow Li_4SiO_4 + CO_2$. Phase pure Li_4SiO_4(JCPDS-37-1472) was formed above 650^{o}C which was confirmed by the XRD graph (fig.5.5). On further increase of calcination temperature above 650^{o}C, Li_4SiO_4 is the only phase till 750^{o}C. However the TG curve indicated continuous mass loss of about 10% after 750^{o}C which could be due to burning of the carbonaceous matter or li-evaporation form the system. The crystallite size obtained in SCR sample at 650^{o}C was 131nm which gradually increased with temperature.

5.3 Thermal and phase analysis of SSR derived Li_4SiO_4 powder

For the sake of comparison $Li_4SiO_4$was also prepared using solid state method following the conventional method of mixing, grinding and calcining.

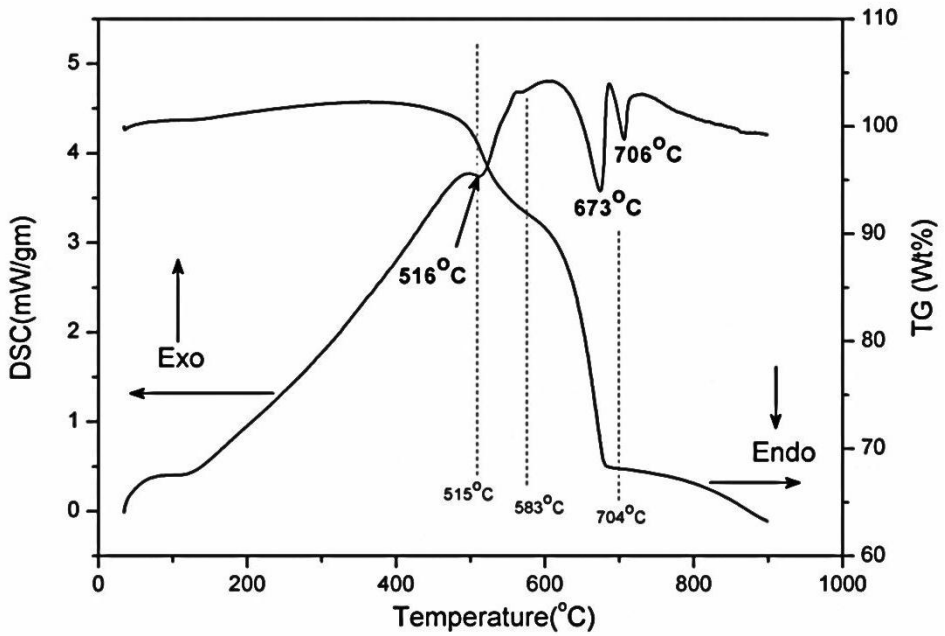

Fig. 5.6: DSC-TG plots of the stoichiometric mixture of Li_2CO_3 and Silica powder (White Ash from RHA) (SSR samples)

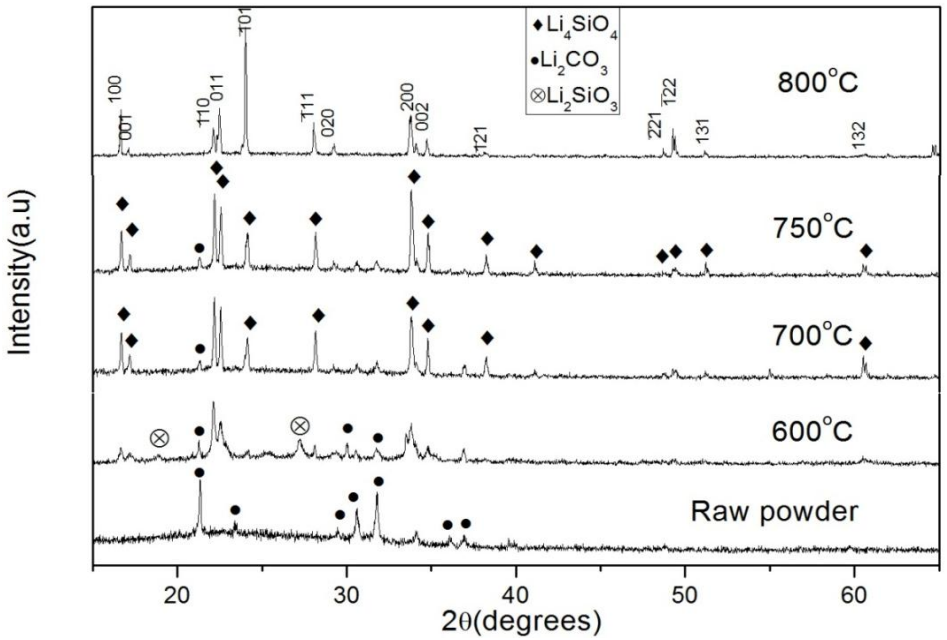

Fig. 5.7: XRD pattern of the stoichiometric mixture of Li_2CO_3 and Silica powder (White Ash from RHA) calcined at different temperature

In order to understand the phase formation behavior of Li_4SiO_4in Solid State Route (SSR) samples, dried precursor powder [mixture of $Li_2CO_3$and Silica powder (White Ash from RHA)with Li: Si molar ratio of 4] was analyzed by DSC-TG. According to TGA plot,the sample shows an overall weight loss of about 37% from 515^oC to 900^oC. There existed three mass loss of about 11%, 22% and 5% in temperature range of 515 - 583^oC,583- 704 ^oC and 704 - 900^oC respectively. DSC results of SSR samples showed that there was one small endothermic peak at 516^oC. It could have been due to formation of Li_2SiO_3 and release of carbon dioxide which is confirmed from XRD plot (fig.5.7) at 600^oC. The sharp endothermic peaks at 673^oC refer to the absorption of more heat for the formation of Li_4SiO_4(by the reaction of $Li_2SiO_3$and Li_2CO_3) as confirmed from XRD plot (fig.5.7) at 700^oC and evolution of carbon dioxide. Another endothermic peak is seen at 706^oC which may be due to the melting of Li_2CO_3 (m.p. of Li_2CO_3 is 723 ^oC). However, further decomposition of Li_2CO_3 appears to favor the formation of Li_2SiO_3. Subsequent conversion to Li_4SiO_4 of Li_2SiO_3 is dependent on the decomposition of Li_2CO_3.

In Fig. 5.7, at 750^oC the intensities of Li_2CO_3 peaks were however very weak, indicating low content of Li_2CO_3 phase in the products. On further increase of temperature, at 800^oC, the crystalline peaks of Li_2CO_3 disappeared and only peaks of Li_4SiO_4 remained, which demonstrated phase pure of Li_4SiO_4.It can be concluded that Li_4SiO_4 was formed via formation of Li_2SiO_3. The crystallite size obtained for solid state route at 800^oC was 247.16nm.

Accordingly, the synthesis process of Li_4SiO_4 using SSR between Li_2CO_3 and SiO_2 may be described as following two steps: [5]

$$Li_2CO_3 + SiO_2 \rightarrow Li_2SiO_3 + CO_2 \ (515\text{-}583^oC) \qquad (5.2)$$

$$Li_2CO_3 + SiO_2 \rightarrow Li_2SiO_3 + CO_2 \ (583\text{ -}704^oC) \qquad (5.3a)$$

$$Li_2CO_3 + Li_2SiO_3 \rightarrow Li_4SiO_4 + CO_2 \ (704\text{ - }900^oC) \qquad (5.3b)$$

5.4 ICPS analysis of powder samples

Inductively Coupled Plasma Atomic Emission Spectrometer (ICPS) analysis showed the presence of different elements for SCR samples. The results were summarized in Table 5.1. The table showed the presence of Li and Si with trace amount of Fe, Ti and Na which might have come from the source of silica (from RHA) that has been used for the synthesis of SCR samples. Chemical purity of silica powder was 99.87%. The presence of 0.13 wt % of alumina may have come from the source of Li_2CO_3.The theoretical weight percentage of each element in Li_4SiO_4 was also matched with the mean weight percentage of the constituent elements by ICP-AES analysis.

Constituents	Mean % Wt.	Method used
Si	24.03	Volumetry
Al	0.13	ICP
Fe	0.03	ICP
Ti	0.01	ICP
Na	0.10	ICP
Li	22.09	ICP

Table 5.1: Table showing the elemental analysis ofSCR samples

ICP-AES analysis is important to find out the presence of other elements (like Al, Fe, Ti, Na etc) which could hamper the tritium release. The element Al, which absorbs the high energy neutron, affects the generation of tritium. But still it is in allowable limit.

5.5 Characteristics of Li_4SiO_4 powder

Phase pure Li_4SiO_4powder prepared by SSR and SCR were analyzed using BET, Nano-Analyzer and SEM which are presented in fig.5.8, fig.5.9 and fig.5.10 (a & b) respectively.

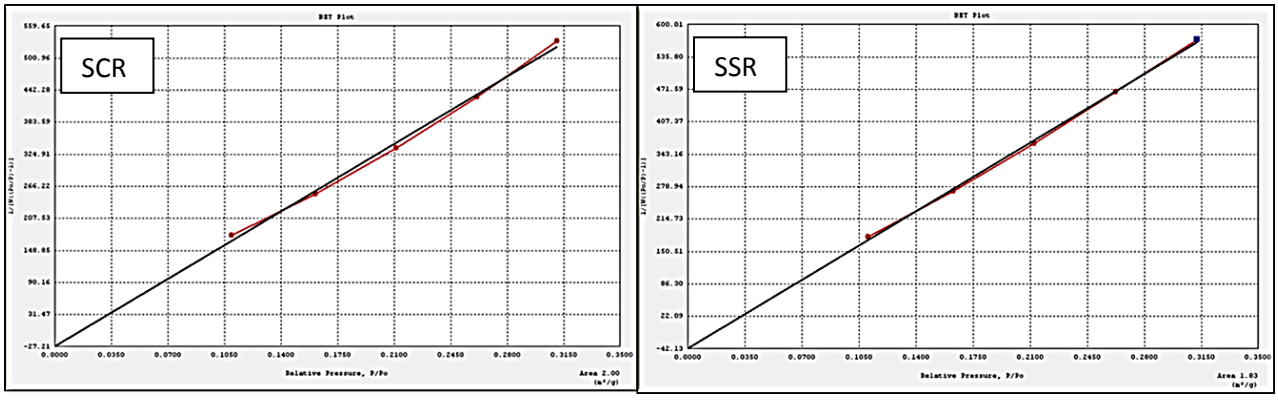

Fig.5.8: BET Plots for SSR and SCR derived Li_4SiO_4 powder

Fig.5.8 shows five point BET plots for SSR and SCR samples.It was found that Li_4SiO_4powder had surface area 1.83m^2/g and 2.03m^2/gmfor SSR and SCR samples respectively.

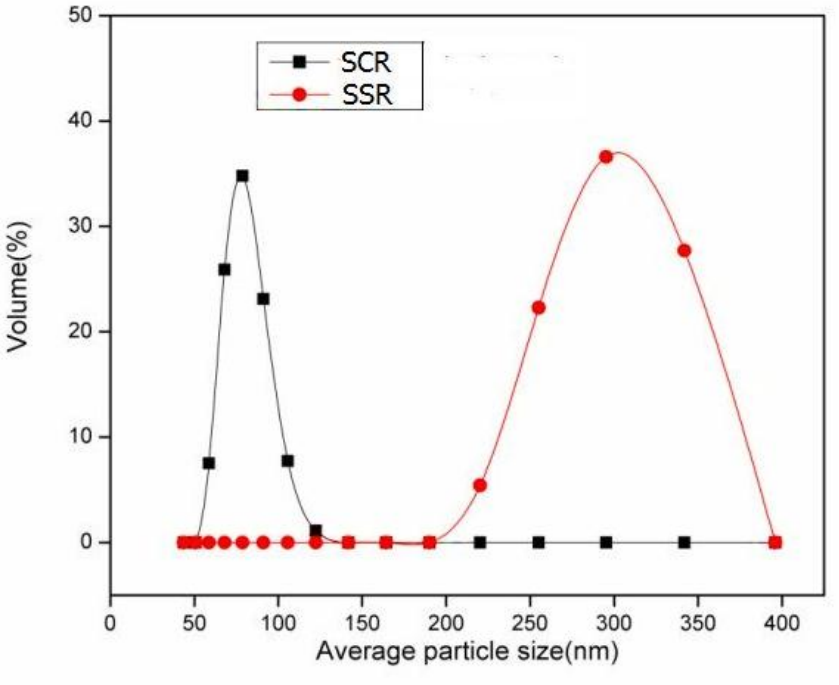

Fig.5.9: Particle size distributionof SSR and SCR samples

The average particle size of Li_4SiO_4 (SSR and SCR) samples were compared in fig.5.9. SSR derived Li_4SiO_4powder had a broad particle size distribution range with 65 vol% of the particle lying in the range 250-450 nm. This may be due to the hard agglomerates present in solid state powder. The mean particle size calculated to be 0.3 µm. The particle size distribution for SCR derived Li_4SiO_4powder was narrow with 60 vol% of the particle lying in the range 50-150 nm. The mean particle size calculated to be ~90 nm.

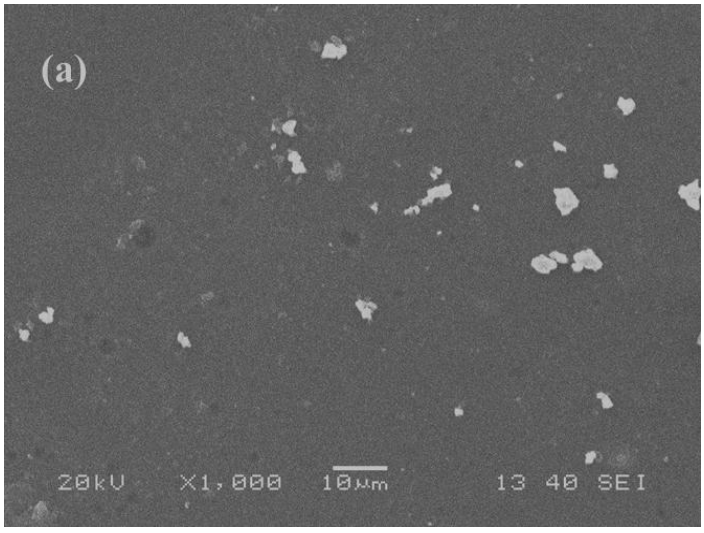

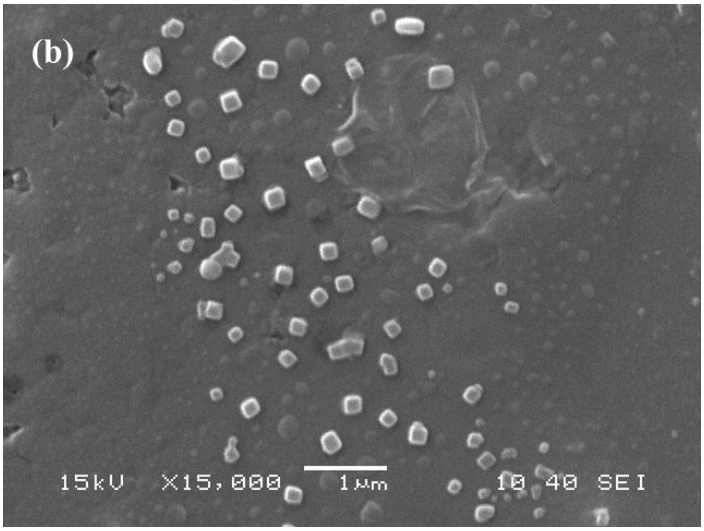

Fig. 5.10: SEM micrograph showing dispersed Li_4SiO_4 (a) SSR and (b) SCR samples

SEM micrographs of SSR derived Li_4SiO_4powder was shown in fig.5.10(a) which indicated large particle size ranging from 0.5 to 5µm. The large particle size could be attributed to the hard agglomerates formed due to calcination at 800^oC. Moreover the particle shape was non-uniform. Fig.5.10(b) showed the SEM image of Li_4SiO_4SCR powder samples. The average particle size (~80nm) of SCR powder samples were smaller than the SSR derived Li_4SiO_4powder which could be attributed to the low temperature synthesisof SCR powder.The particles wereuniformand cubical in nature.

5.6 Compaction behavior of calcined powder

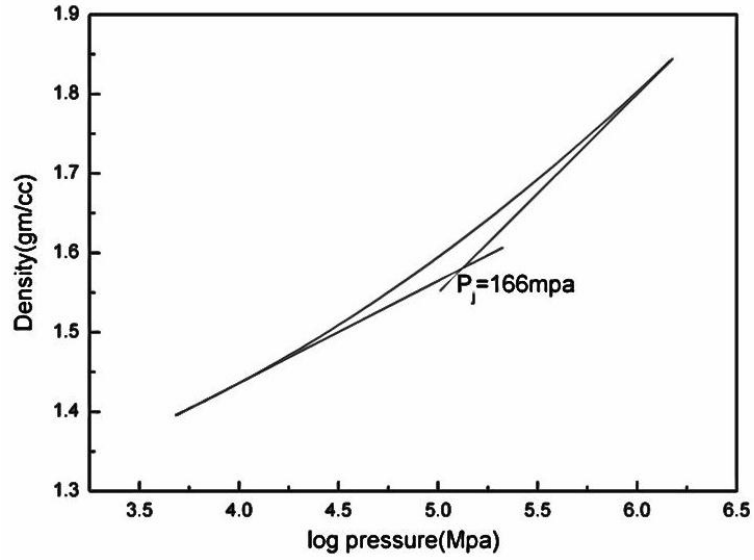

Fig.5.11: Compaction behavior of the calcined Li_4SiO_4 (SSR samples)

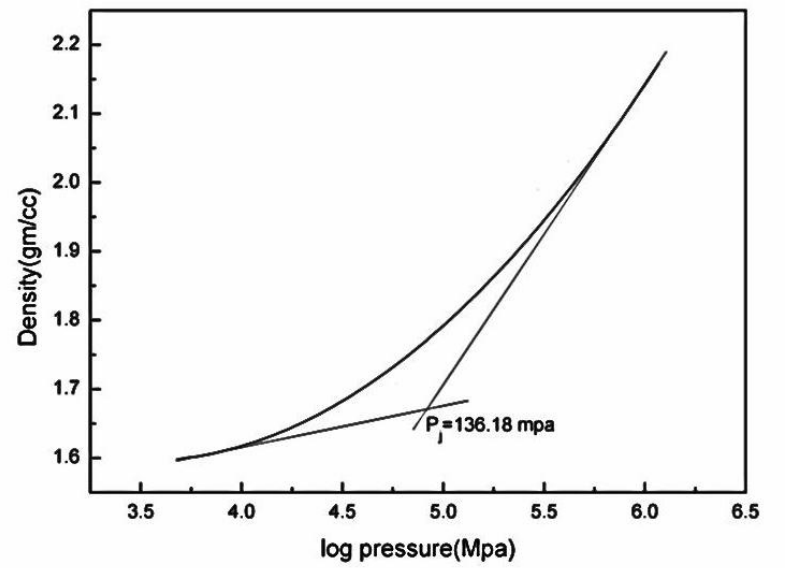

Fig.5.12: Compaction behavior of the calcined Li_4SiO_4 (SCR samples)

Figure 5.11 and 5.12 shows the semi logarithmic plot of compaction pressure as a function of density of the green compacts for as prepared calcined SSR and SCR powder. The graph of green density vs log (compaction pressure) provided important information about the powder compaction behavior. Usually, compaction of ceramic powders took place in two stages:

Stage-I Granule flow and rearrangement

Stage-II Granule deformation combined with granule densification.

The crushing strength (P_j) of particles was the intersection of the two linear segments and the P_j value varied with size, shape and extent of particle breakage from brittle fracture.

Stage-I took place at lower pressure, where a small amount of sliding and granule rearrangement took place. Stage – I results in a slight densification above the fill density. Stage-II occurred above P_j and began with granule deformation, which subsequently shifted to granule densification process. The dependence of agglomerate break point P_j on the granule parameter during stage –II compaction could be described by the following equation.

$$\rho_{compact} = \rho_{fill} + M \log \frac{P_a}{P_j} \qquad (5.4)$$

where, $\rho_{compact}$ was the compact density at an applied pressure P_a, $\rho_{fill}$was the filled density and 'M' was the compaction constant that depends on the deformability and densification characteristics of the granules.The critical pressure (P_j) or the agglomerate break point

denoted the strength of the agglomerate. The lower was the agglomerate strength; the softer will be the agglomerate which will easily break under compaction load leading to better compaction and high green density. The as prepared SSR prepared powder showed higher P_j value (166 MPa) than SCR calcined powder (136Mpa).It was observed that powders containing high density granules might produce a high compact density with a lower value of '*M*' (up to 5). Low density granules, on the other hand have '*M*' in the range of 7-10. For the SSR and SCR prepared Li_4SiO_4 powder '*M*' was 6.3 and 2.9 respectively which indicate that theSCR powder has high-density granules [6].

5.7 Densification behavior of green compacts

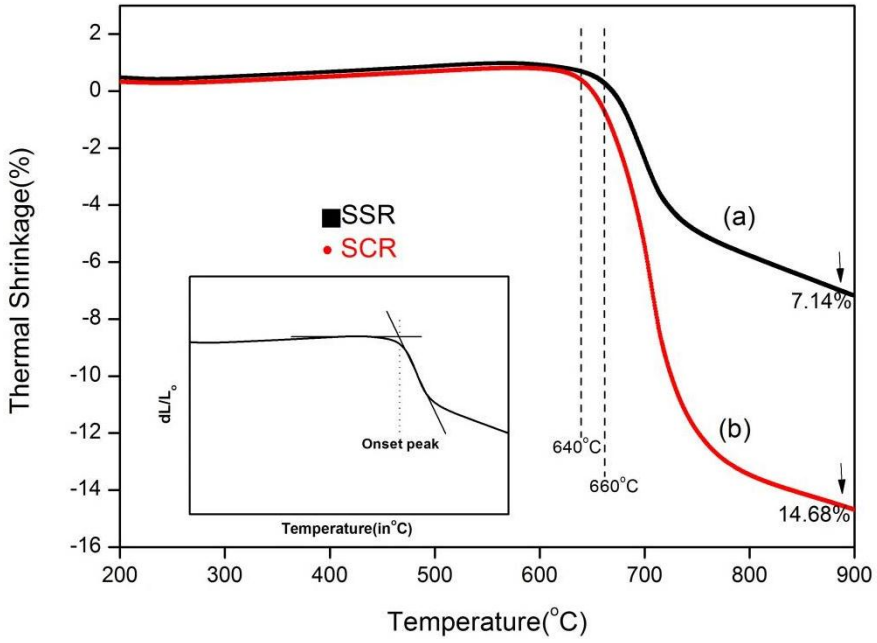

Fig.5.13: Thermal shrinkage of Li_4SiO_4powder compact (a) SSR and (b) SCR samples

Fig. 5.13 represents the thermal shrinkage behavior of Li_4SiO_4 powder compact of SCR and SSR. The convention for determining the onset peak was to extend the straight line portions of the base line and the linear portion of the upward slope, marking the intersection. The convention was similar for locating T_g, the glass transition temperature [7]. The onset temperature for SSR and SCR samples were 640^{o}C and 660^{o}C respectively. As observed from the dilatometric curve, a slight thermal dilation was found below 640^{o}C and a rapid decrease of the length occurred above 640^{o}C for SSR Li_4SiO_4 samples. Similar pattern was observed for SCR Li_4SiO_4 samples below and above 650^{o}C.The linear shrinkage of the bar

prepared by SCR was about 14.68 % double that of the SSR bar (7.14%), indicating much higher sinterability of the Li_4SiO_4 powders obtained by the SCR. The shrinkage was almost complete by 900^oC for both SSR and SCR samples. However further increment in temperature could not be done because the samples (SSR and SCR) got stuck with the push rod of the dilatometer which limited our measurement. Dilatometer study gave an indication that sintering of Li_4SiO_4 samples (SSR and SCR) could be possible in a temperature range of 850 - 950^oC.

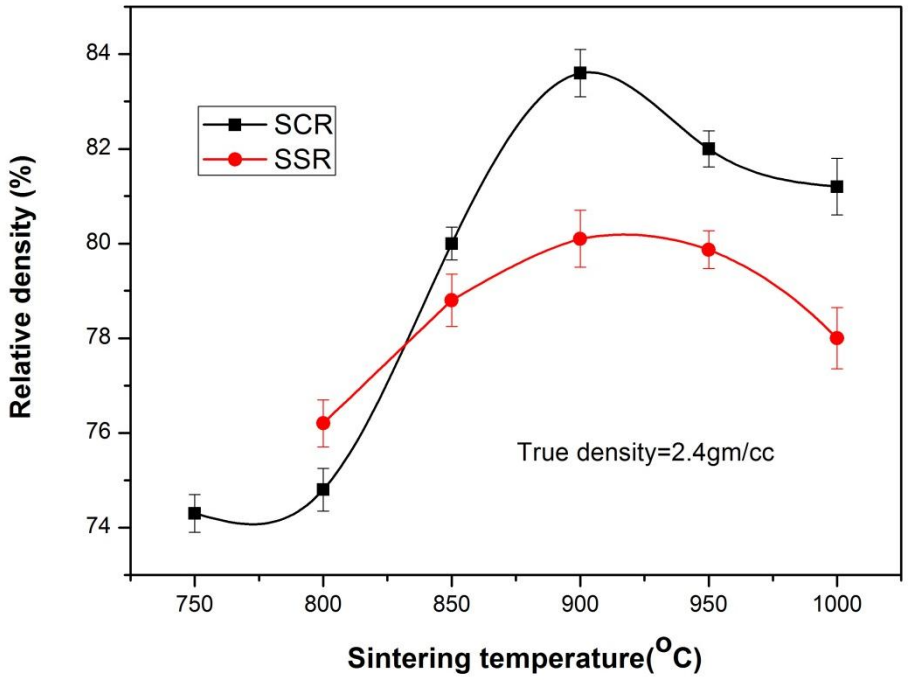

Fig.5.14: Variation in relative density with sintering temperature for SSR and SCR sintered pellets

Fig. 5.14 shows the variation in relative density with the sintering temperature. The temperature was varied from 750 - 1000^oC and 800 - 1000^oC in the interval of 50^oC for SCR and SSR derived samples respectively. The sintering is done at a heating rate of 2^oC/min with a soaking period of 4 hrs. From the figure, it is evident that the bulk density of the pellets [as a % of theoretical density of Li_4SiO_4 (2.4 g/cm^3)] increased with increasing temperature up to 900^oC followed by a decrease with further increase in temperature. Higher density in SCR samples could be attributed to smaller particle size and high reactivity of the solution combustion derived powder. Lowering of sintered density above 900^oC could be attributed to the Li-evaporation(weight loss more than 8.5% above 900^oC) and formation of secondary

phase (Li_2SiO_3) at higher temperature. The maximum density attained inSSR and SCR samples was 1.92 gm/cc (80.12% RD) and 2.004gm/cc (83.6% RD) at 900^{o}C respectively.

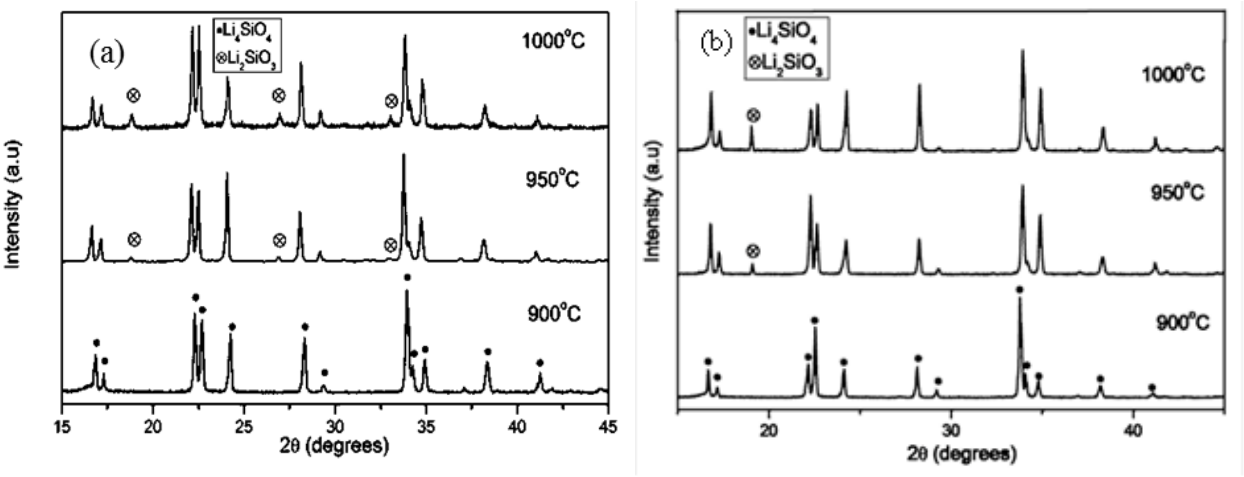

Fig.5.15: XRD of Li_4SiO_4 at different sintering temperature for (a) SCR (b) SSR pellets

Fig.5.15 shows the XRD patterns of SCR and SSR ground pellet which contains Li_2SiO_3 phase when sintered above 900^{o}C. However the intensity of Li_2SiO_3peaks gradually increased from 6 – 8 % and 8 – 10 % for SCR and SSR sintered samples at 950 – 1000^{o}C respectively.

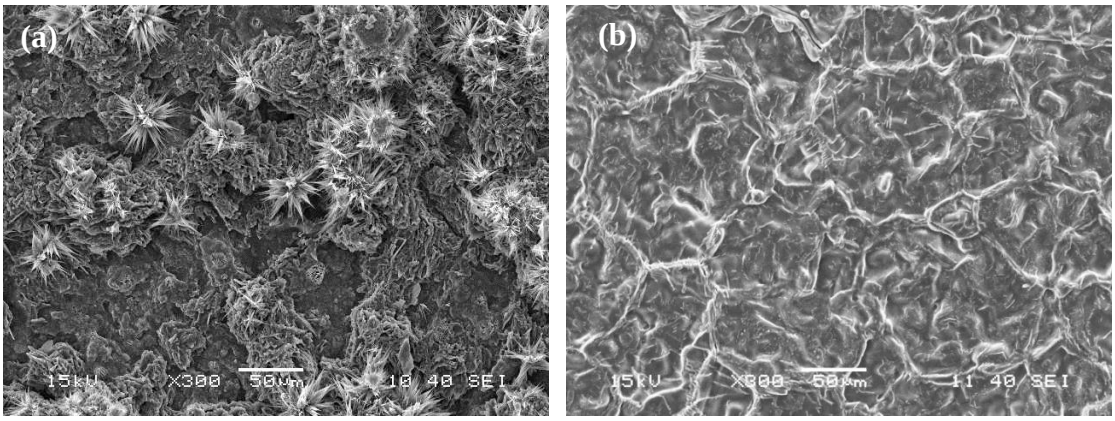

Fig.5.16:SEM of Li_4SiO_4pellets sintered at (a) 950^{o}C and (b) 1000^{o}C

Fig. 5.16 shows the SEM micrographs of the Li_4SiO_4sintered pelletsat 950^{o}C and 1000^{o}C for SCR derived powder. Similar SEM picture were obtained for SSR derived powder. In fig.5.16 (a) needle or spike like structure were observed which could be identified to be Li_2SiO_3. $Li_2SiO_3$is a silicate which has a linear $(SiO_3)^{2-}$structure [8].The needle like structure

could be produced due to the union of several Li_2SiO_3 chains i.e. each Li_2SiO_3get connected to each other [9]-[10]. Cross linking of these needle like structures produces a porous structure which reduces the density above 900^oC for both SCR and SSR sintered samples. Above 950^oC sufficient amount of liquid phase formed which densified surface but finally density reduced due to non removal pores.

5.8 Various sintering methods adopted to improve density

It was seen in sec 5.7 that the maximum density achieved was 83.6 % RD. It was also found that Lithium sublimation was inevitable in various lithium ceramics [11]-[16]. Li_2O sublimation may have been one of the reasons for the huge weight loss occurring above 900^oC.Sublimation takes place by the following reaction:

$$Li_4SiO_4 \xrightarrow{>900^oC} Li_2SiO_3 + Li_2O \qquad (5.5)$$

In order to minimize the lithium loss from the (SSR & SCR) sample above 900^oC and to increase density above the achieved density (2.006gm/cc), following methods were tried during sintering of lithium orthosilicate at 900^oC:

i. Sintering methods -I Pellets were sintered in presence of Li_2CO_3.
ii. Sintering methods -II Pellets were sintered covering with Li_4SiO_4 powder in a closed crucible.
iii. Sintering methods -III Li_4SiO_4 containing excess Li (10%/20%/30%) were prepared and later on Li_4SiO_4 pellet was sintered on the bed of these excess Li batches.

The densities of sintered Li4SiO4 pellets by different sintering techniques were presented in Table 5.2. From the table it was observed that slight increase of about 2% in density took place for sintering -III.

Sintering method	**Relative density(%)**
I	83.13
II	could not be measured due to reaction with the surrounding powder
III (20% excess Li)	85.18

Table 5.2: Change in density for different sintering technique

5.9 Kinetic Analysis for initial stage of sintering

The initial stage consists of fairly rapid inter-particle neck growth by diffusion, vapor transport, plastic flow, or viscous flow. The large initial differences in surface curvature are removed in this stage, and shrinkage (or densification) accompanies neck growth for the densifying mechanisms[17].

5.9.1 Determination of sintering mechanism

Several theoretical approaches have been used to analyze the densification process during sintering, including the use of analytical models, scaling laws, and numerical simulations. These approaches, particularly the analytical models, have been criticized because the drastic simplifications assumed in the models make them unsuitable for quantitatively predicting the sintering behavior of real powder systems. Commonly, the models assume uniform packing of monosize spherical particles, the occurrence of a single mass transport mechanism, and no grain growth. At best, they provide only a qualitative understanding of sintering. In spite of these shortcomings, the role of the theoretical models in the development of our understanding of sintering should not be overlooked.

Looking into the difficulties arising in achieving density more than 85%, the dilatometer curve is analyzed kinetically. The kinetics of initial stage of sintering for non-isothermally treated dilatometer curve was analyzed. The theoretical models that have been discussed in literature are based on coalescence of two tangent spheres. In order to find out which sintering mechanism (Surface transport and bulk transport sintering mechanism) was operating during the initial stage the dilatometer curve at 3^{o}C/min was analyzed.

The generalized form of neck growth can be expressed from the two-sphere densification/sintering model [17].

$$\left(\frac{X}{R_P}\right)^n = \frac{Bt}{R_P^m} \tag{5.6}$$

where, X is the neck radius, Rp is the particle radius, t is the time, m and n are constants and the value of m and n depended on the kinetic mechanism of the initial stage of sintering, $B = B_oT^a$, where B_0 corresponds to the combined material and numerical constants and is related to the temperature (T) through the Arrhenius law. The exponent n (kinetic constant) of Eqn.

(5.6) identifies the sintering mechanism. The value of n for different mechanism and the corresponding values of the temperature exponent 'a' have been given in Table 5.4.

The neck growth and the shrinkage for the densification can be correlated by Eqn. 5.7, where L_o is the initial dimension of the green compact and ΔL is the shrinkage at time t.

$$\frac{\Delta L}{L_0} = \left(\frac{X}{2R_p} \right)^2 \tag{5.7}$$

Equation (5.6) and (5.7) can be combined to yield Eqn. (5.8)

$$\frac{\Delta L}{L_o} = \left(\frac{B_o T^a t}{2^n R_p{}^m} \right)^{2/n} \tag{5.8}$$

and this describes the densification behavior for isothermal conditions.

Kinetic Model	**a**	**n**
Viscous flow	0	2
Plastic flow	-1	2
Volume diffusion	-1	5
Grain boundary diffusion	-1	6
Evaporation condensation	-3/2	3
Surface diffusion	-1	7

Table 5.3: Dependence of frequency factor with temperature corresponding to the kinetics models used in literature

The time derivative of Eqn. (5.8) is

$$\frac{d(\Delta L/L_0)}{dt} = \frac{d}{dt}\left[\frac{B_o T^a t}{2^n R_p{}^m} \right]^{2/n} = k\left(\frac{\Delta L}{L_0} \right)^{1-n/2} \tag{5.9}$$

where, $k = B_0 T^a / 2^{n-1} n R_p{}^m$. B_0 can be expressed by the Arrhenius type relationship

$$k = Ae^{-Q/RT} \tag{5.10}$$

where, Q is the activation energy and $A = A_0 T^a$. The pre-exponential factor (A) of the Arrhenius equation is dependent on the exponent '*a*'describing the dependence with the

absolute temperature *T*. Substitution of Eqn. (5.10) into eqn. (5.9) results in the following equation.

$$\frac{d(\Delta L/L_0)}{dt} = A_0 T^a e^{-Q/RT}\left(\frac{\Delta L}{L_0}\right)^{1-n/2} \tag{5.11}$$

Equation (5.11) describes the time rate of shrinkage ($\Delta L/L_0$) at a certain temperature and gives the generalized expression applicable for both isothermal and non-isothermal densification condition [18]-[21].Thus, any set of data $d(\Delta L/L_0)/dt$-T- $\Delta L/L_o$ should fit Eqn. (5.11) independent of the experimental conditions (i.e., isothermal, non-isothermal conditions).

The dilatometric curve obtained from a linear-heating rate ($\beta = dT/dt$), i.e., non-isothermal condition can be described by the Eqn. (5.13) (which is obtained by integrating (5.12) followed by rearrangement).

$$T^2\left(\frac{d(\Delta L/L_0)}{dt}\right) = \frac{2\beta Q}{nR}\left(\frac{\Delta L}{L_0}\right) \tag{5.12}$$

The sintering activation energy and the mechanism of densification can be determined from the value of the Q and n respectively. The linear plot of $T^2\left(\frac{d(\Delta L/L_0)}{dt}\right)$ vs $\left(\frac{\Delta L}{L_0}\right)$ as a function of heating gives an idea of $\left(\frac{Q}{n}\right)$ ratio; however, the individual value is difficult to determine. In order to find the densification mechanism and densification activation energy, one needs to know the value of either Q or n. The simultaneous determination of Q and n is only possible using the modified eqn. (5.9).

Freeman and Carroll[22]proposed that the sintering kinetics could be determined from a single CRH curve by modifying the Eqn. (5.11).

The differentiation of the logarithmic form of Eqn. (5.11) with respect to $d\ ln\ (\Delta L/L_0)$ gives

$$\frac{d\ln\frac{d(\Delta L/L_0)}{dt}}{d\ln(\Delta L/L_0)} - a\left(\frac{d\ln T}{d\ln(\Delta L/L_0)}\right) = -\left(\frac{Q[d(1/T)]}{R[d\ln(\Delta L/L_0)]}\right) + 1 - \frac{n}{2} \tag{5.13}$$

or

$$\frac{\Delta \ln \frac{d(\Delta L/L_0)}{dt}}{\Delta \ln(\Delta L/L_0)} - a\left(\frac{\Delta \ln T}{\Delta \ln(\Delta L/L_0)}\right) = -\left(\frac{Q[\Delta(1/T)]}{R[\Delta \ln(\Delta L/L_0)]}\right) + 1 - \frac{n}{2} \quad (5.14)$$

For a fixed value of '*a*', the plot of LHS of Eqn. (5.13) or (5.14) against d(1/*T*)/d ln ($\Delta L/L_0$) or $\Delta(1/T)/\Delta \ln (\Delta L/L_0)$ respectively, yields a straight line as shown in fig.5.17, whose slope is *Q/R* and *(1-n/2)* is the intercept. Thus, *Q* and *n* can be simultaneously determined from this model (Eqn. (5.13) or (5.14)) using a single dilatometric curve. However, the parameter '*a*'is to be assumed from the Table-5.4 for fitting into these equations. The value of Q has been calculated in sec.5.9.2 along with different heating rates. The value of *n* was found to be 1.7. According to Table 5.4, n = 1.7 (~2) indicate that the densification is governed by viscous flow.For this mechanism, matter transport was assumed to be governed by Frenkel's energy balance conceptwhere rate of energy dissipation by viscous flow will be equal torate of energy gained by reduction in surface area[23].

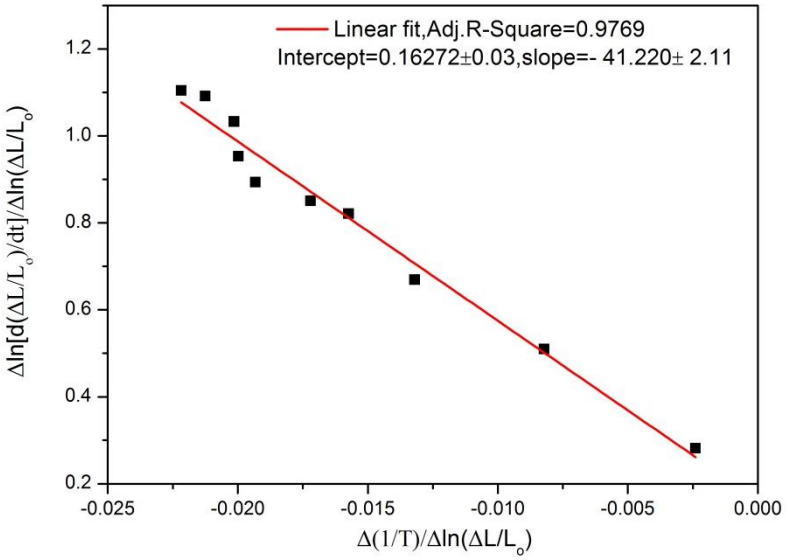

Fig.5.17: Plot of data taken from dilatometry in agreement with Eq.5.13

5.9.2 Determination ofsintering activation energy

Heating rate is an important considerations in materials investigations.The kinetic analysis of initial stage sintering was limited to the fractional shrinkage ≤ 3 %, implying densification without grain growth.The initial stage sintering kinetics for Li_4SiO_4 for different heating rates has been analyzed from dilatometric studies using Eqn. 5.12.The shrinkage data ($\Delta L/L_0 \leq 3$

%) has been obtained from the non-isothermal sintering curve at different heating rate (fig. 5.18).

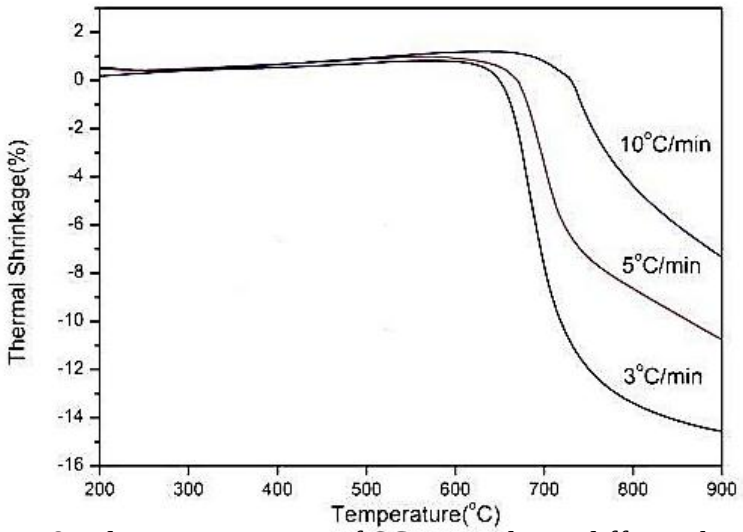

Fig.5.18:Dilatometric curves of SCR samples at different heating rate

The graph of $T^2\left(\frac{d(\Delta L/L_O)}{dt}\right)$ vs $\left(\frac{\Delta L}{L_O}\right)$ as a function of heating rates yields a straight line (Fig.5.19). Thus, the activation energy for densification could be calculated from the Q/n ratio obtained by analyzing the constant rate heating sintering dilatometric curves. The slope, r (regression coefficient) and hence Q/n and activation energy value calculated from the fitted equation has been given in Table 5.4.

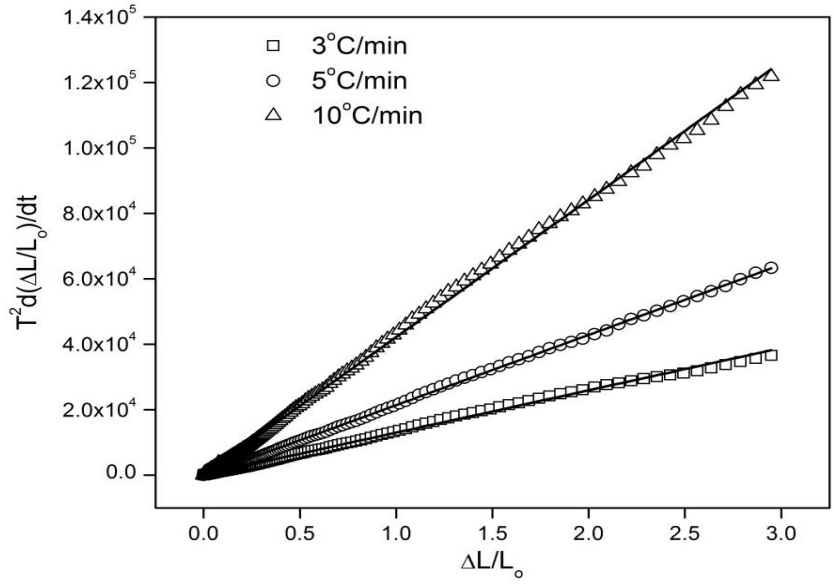

Fig.5.19:Analysis of the Dilatometric curve obtained at different heating rateusing Eq.5.12

Rate (β) °C/min	r	Slope	$\frac{Q}{n}$	Activation energy (KJ/mol^{-1})
3	0.997	12924	17908	35.8
5	0.999	21461	17843	35.68
10	0.999	42012	17464	34.93

Table 5.4: The slopes and Q/n from the Fig.5.23 using Eqn. 5.12

It was found that the sintering activation energy is almost independent with the heating rate.

5.10Effect of heating rate and dwelling time on bulk density

From sec.5.7 and 5.8, it was seen that maximum density achieved was 83.6% of theoritical value and even after adopting different techniques for sintering , the density could be improved to 85% of theoritical value. In this section, the rate of heating as well as the soaking period during sintering process was varied keeping the temperature constant at 900^{o}C. The temperature was constant from the fact that the maximum density was achieved at 900^{o}C for 6 hrs with 2^{o}C/min heating rate.The idea was to observe the density of the sintered smples.

Rate of heating	Soaking period	Relative Density
2^{o}C	30 min	78.2
	1 hr	78.79
	2 hr	79.2
	4 hr	82
	6 hr	**83.6**
3^{o}C	6 hr	82
5^{o}C	6 hr	80
10^{o}C	6 hr	78.78
15^{o}C	6 hr	78.18

Table 5.5:Effect of soaking period and rate of heatingon densificationofSCR derived powderat 900^{o}C

Sintering rate was varied for 3^oC, 5^oC, 10^oC and 15^oC/min keeping the soaking period constant at 900^oC/6hrs. It is observed from the table 5.5 that increase in heating rate decreases the density of the sintered sample and that may be due to decrease in overall firing time at a particular temperature. In another case, the soaking period was varied from 30 min to 6 hr at 900^oC keeping the heating rate constant at 2^oC/min during sintering. An overall 6% increase in density was observed during the variation of soaking period. Increase in dwelling period during sintering resulted in increase in density that may be attributed to the uniform heat distribution for longer dwelling periods. Thus, slow heating rate (2^oC/min) with longer dwelling time was favorable in achieving higher sintered density (~84%).

5.11 Mercury porosimetry of sintered SSR and SCR derived Li_4SiO_4specimens

Hg-Porosimetry analysis has been widely used to estimate the pore size distribution and amount of open porosity in the various ceramics [23]-[26]. Tritium diffusion and release is dependent on the percentage of interconnected open porosity in lithium based ceramics. In order to find the open porosity percentage Hg-Porosimetry analysis of the fractured sintered pellets was used. But prior to measurements of Li_4SiO_4samples, standard silica samples were measured for the pore size analysis.

The Li_4SiO_4 samples (SSR and SCR) sintered at 900^oC/6hrs with 2^oC/min heating rate were taken for Porosimetry analysis. Hg- Porosimetry analysis of SSR derived Li_4SiO_4 (fig.5.20a) revealed that the pore size distribution was multimodal andthe pore diameter varied from 0.5 - 200µm. The SCR derived Li_4SiO_4 fractured pellets (fig.5.20b) showed narrow pore size distributions with pore diameter in the range of 0.2 to 10µm. The total porosity was found to be 23.56% and 30.3 % for SCR and SSR sintered samples respectively.

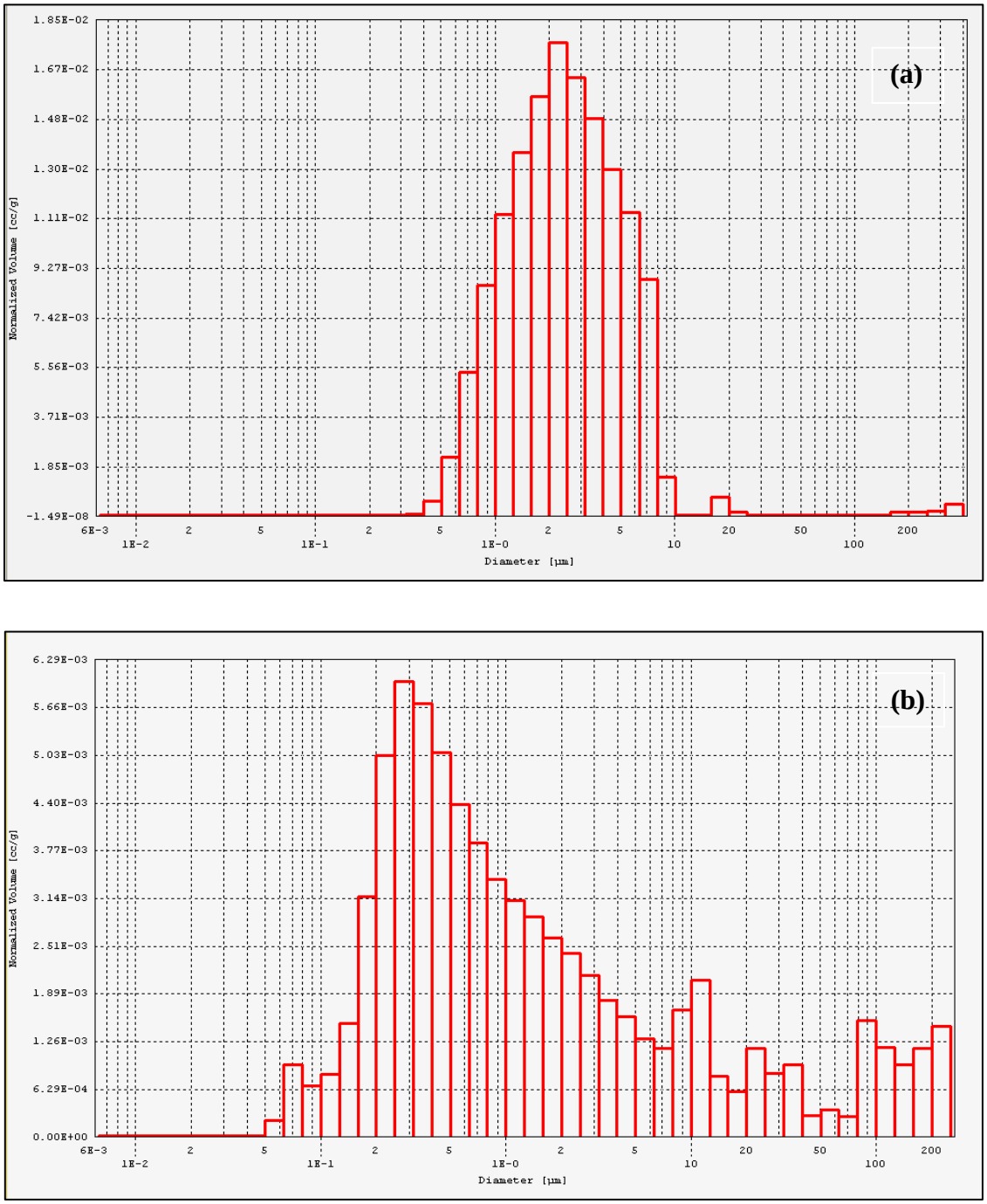

Fig.5.20:Normalized Intrusion volume vs. pore size histogram for (a) SSR and (b) SCR derived Li_4SiO_4 pellets

5.12 Microstructure of sintered specimens

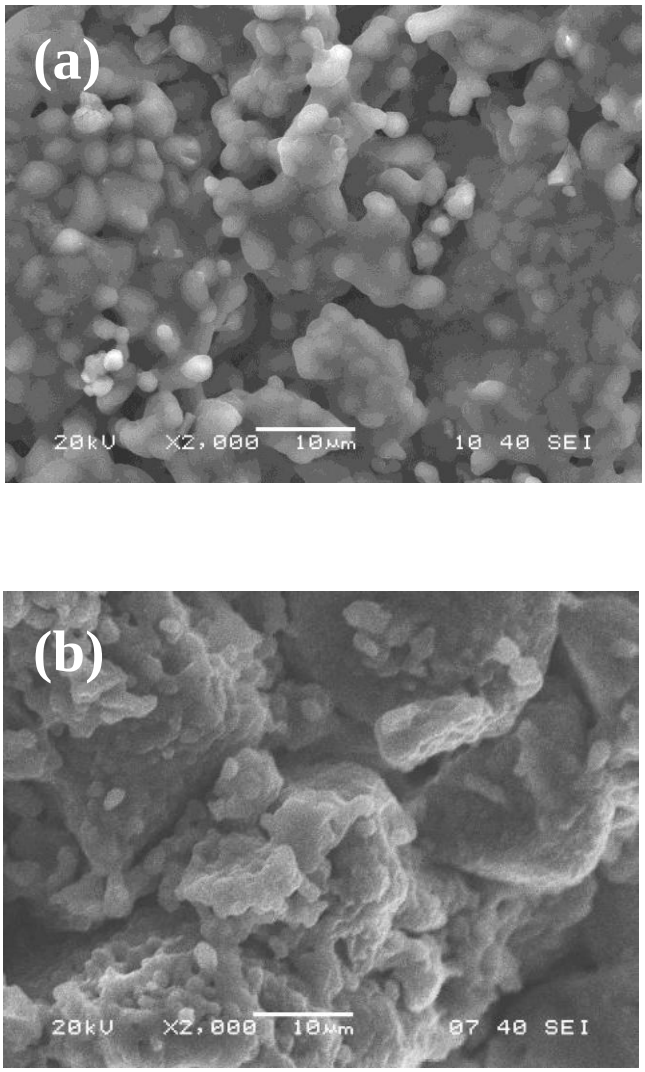

Fig.5.21: Microstructure of (a) as sintered (b) fracture surface of SCR derived sintered (900^{o}C/6hrs) pellet

Fig. 5.21 (a & b) shows the as sintered and fracture surface of 900^{o}C/6hrs SCR pellets. The as-sintered surface showed the presence of open pores which was expected as the density could not be achieved above 85% of RD. The sample contained mostly open pores which were reflected in our porosimetric analysis. The fracture surface (Fig.5.21b) shows that absence of close pore in the structure. Fig.5.21 (a) showed homogenous grain size around 4.1µm with minimum grain size of 2.2 µm and maximum grain size of 6.7 µm and standard

deviation factor is 1.4μm.The values was found out by analyzing the micrograph by ImageJ software.

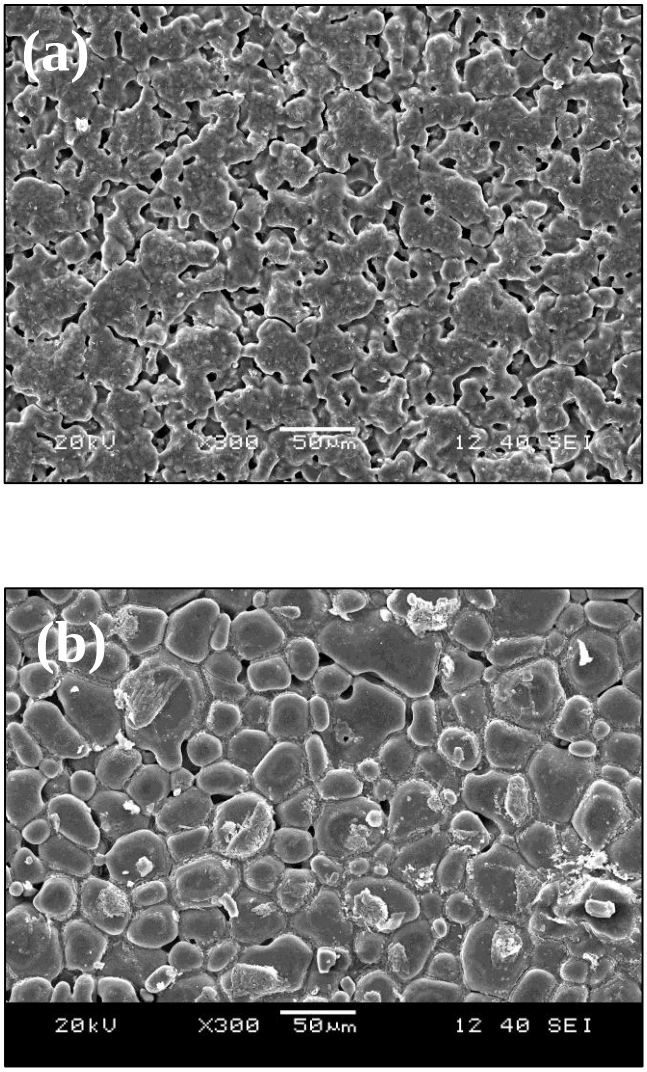

Fig.5.22: Microstructure of as sintered surface of SSR derived Li_4SiO_4 pellets sintered at (a) 900^oC (b) 1000^oC

Fig.5.22 (a & b) shows the microstructure of SSR samples sintered at 900^oC and 1000^oC/6hrs. Fig.5.22a showed as- sintered surface with large grains (50-100μm) and lot of

trapped pores. The large grain size is detrimentalfor tritium release since the tritium ion has to follow a large path in order to come out of the breeder grain. Generally large diffusion path of tritium ion results in entrapment of the said ions in the grain.

5.13 Moisture reactivity of Li_4SiO_4 powder by FTIR analysis

The hygroscopic nature of lithium ceramics is a critical factor in the materials selection for the design of ceramics breeders, due to their moisture affinity, which can produce a decrement in its properties due to the presence of sorbed water[26]-[28]. The absorption of water was found to decrease Li^+ hopping frequencies by a factor of 3 to 4 [29].Thus, the exposition of Li_4SiO_4 to water vapor may affect its overall performance.

SCR derived Li_4SiO_4sintered ground pellets were taken for FTIR Analysis.

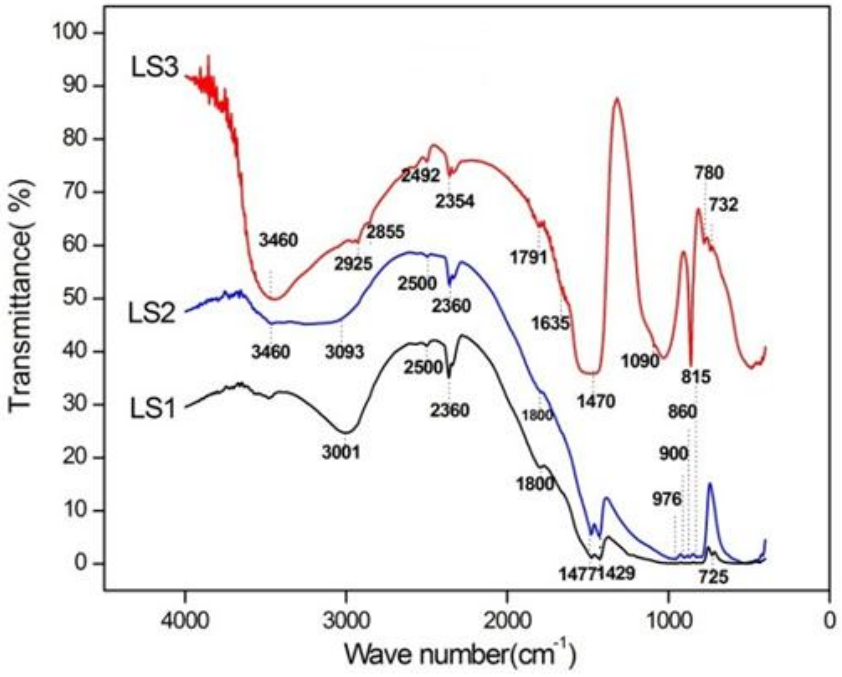

Fig.5.23: FTIR analysis of SCR derived Li_4SiO_4 kept at different humidity

LS1- Sintered Li_4SiO_4powder kept in drier at 110^oC for overnight.

LS2-Sintered Li_4SiO_4powder kept in 94-95% relative humidity for a day.

LS3- Sintered Li_4SiO_4powder kept in 94-95% relative humidity for a week.

In LS2 and LS3, the broad band 3460 cm^{-1} is due to stretching vibration of free –Si-O-H, structured –Si-O-H and -O-H bond [30]. Very recently it is reported [31] that peaks at 3460$cm^{-1}$was due to vibration of Li-OH bonds asit was assumed that the majority of H^+ ions were attracted to the Li sites generating the vibrational mode of Li-OH−. The intensity of absorption peak at 3460cm^{-1} of LS3 was higher when compared to LS1 or LS2 and is due to more adsorption of water molecules on Li_4SiO_4 surface for LS3 samples.

A strong stretching absorption peak is found at 3001$cm^{-1}$for LS1 which was identified to be of –C-H. However, the intensity of –C-H absorption peak at 3093$cm^{-1}$for LS2 grew weaker and finally disappeared in LS3. Rather in LS3, two new small absorption peaks at 2925cm^{-1} and 2855cm^{-1} of LS3 appeared which were attributed to the Si-OC_2H_5 group [32]. The origin of these peaks could be due to the exposure of LS3 sample to humidity environment (containing CO_2) for a long period (1week). The C-H stretching bond may have been formed due to reaction between $Li_4SiO_4$and absorbed CO_2 from air. The presence of C-H bonds is also evident by the presence of double absorption peaks at 2340cm^{-1} and 2360cm^{-1} for LS1 and LS2 respectively. However, in LS3, stretching peak of –C-H was shifted to 2354cm^{-1}[33] .The absorption peak at 2500cm^{-1} for LS1, LS2 and 2492cm^{-1} for LS3 may be due to the O-D bond stretching [34].Two weak absorption peaks at 1800$cm^{-1}$and 1791cm^{-1}were seen for LS2 and LS3 respectively which were attributed to Carboxyl groups. The small absorption peak at 1635cm^{-1} in LS3 sample was assigned to the bending of H-OH bond of water molecules adsorbed on the surface [35].The presence of absorption peak (at 1477cm^{-1}) in all cases were attributed to the asymmetric deformation of –CH_3[36]. The main absorption bands of Li_2CO_3were observed at 1477 cm-^{1}, 1470cm^{-1} and 1429cm^{-1} for anti-symmetric –C-O stretching vibrations. All these are feature of carbonate ion [36]. LS3 showed the presence of small absorption peak at 1090cm^{-1} which was identified to be of Si-O-Si symmetric bond stretching vibration [30]. LS2 revealed the presence of two absorption peaks at 860cm^{-1},815cm^{-1} and LS3 at 863cm^{-1}which were of strong stretching vibration of -Si-OH [38].LS2 showed a unique peak at 976 cm^{-1} which correspond to Si-O symmetric stretching vibration [30]. A weak absorption peak was seen at 900cm^{-1} for LS2 samples which were due to Si-O- with one Non- bridging oxygen atoms per SiO_4 tetrahedron [39]. It could be interpreted that on long exposure of $Li_4SiO_4$to humid environments forced the breakdown of –Si-O-Si- and helped in the formation of weaker links of Si-O- bonds with water [40].

LS1 Absorption Peak (cm^{-1})	**LS2** Absorption Peak (cm^{-1})	**LS3** Absorption Peak (cm^{-1})	**Nature of Peak**	**Identification**
	3460	3460	Stretching vibration	O-H bond from silanol groups and Li-OH
	3093.82		Stretching	-C-H
3001.24				
		2925	Stretching	$Si\text{-}OC_2H_5$
		2855		
2500	2500		Stretching, very broad	O-D
		2492		
2360	2360		Stretching	-C-H
		2354		
2340	2340			
1800	1800		Weak stretching	-C=O
		1791		
		1635	Bending	H-OH
1477	1477	1470	Asymmetric deformation, Antisymmetric stretching	$-C\text{-}H_3$
1429	1429			-C-O
		1090	Asymmetric stretching	Si-O-Si
	976		Symmetric stretching	-Si-O
	900			-Si-O-NBO
	860	863	Strong stretching	-Si-OH
	815			

Table 5.6:Table showing the peak identification and its nature of LS1, LS2 and LS3 samples

5.14 Electrical conductivity measurement

There had been a quantitative similarity between lithium movement and tritium migration in solid breeder materials[41].Fig.5.24 (a) & (b) shows complex plane impedance plots of the SCR and SSR derived sintered Li_4SiO_4 pelletsrespectively at three different measurement temperatures, on heating from the room temperature to 400^oC in air (measured impedance data were converted to specific data taking into account the geometrical shape of the sample).At 200^oC, a slightly depressed semicircular arc is seen next to the coordinate origin. At a higher temperature of 400^oC, a second very small arc comes into play in the low frequency region.The data points of the 200^oC and other temperature arc were fitted using the CNLS fitting routine LEVMW [42]. A simple equivalent circuit, describing symmetric depressed semicircular arcs, is given by the so called distributed element ZARC (Cole–Cole response) which consists of aresistance R in parallel to a CPE element. The CPE impedance is given by $Z(\omega)=A^{-1}\ (i\omega)^{-\alpha}$, ω is the angular frequency, A and α are real constants and $i=(-1)^{0.5}$[43]. The range of α is $0\leq\alpha\leq1$; the CPE acts like a capacitor with a some kind of capacitance. For $\alpha=1$, an ideal semicircle occurs with the center on the Z' axis and the mentioned circuit is given by a resistance R in parallel to a capacitance C.The semicircle at higher frequency side indicates effect of grain conduction and at low frequency side at high temperature reflects either the effect of grain boundary or due to electrode effect. If Li^+ ions are the only charge carriers, semicircle in the high-frequency region can be concluded due to the bulk material.

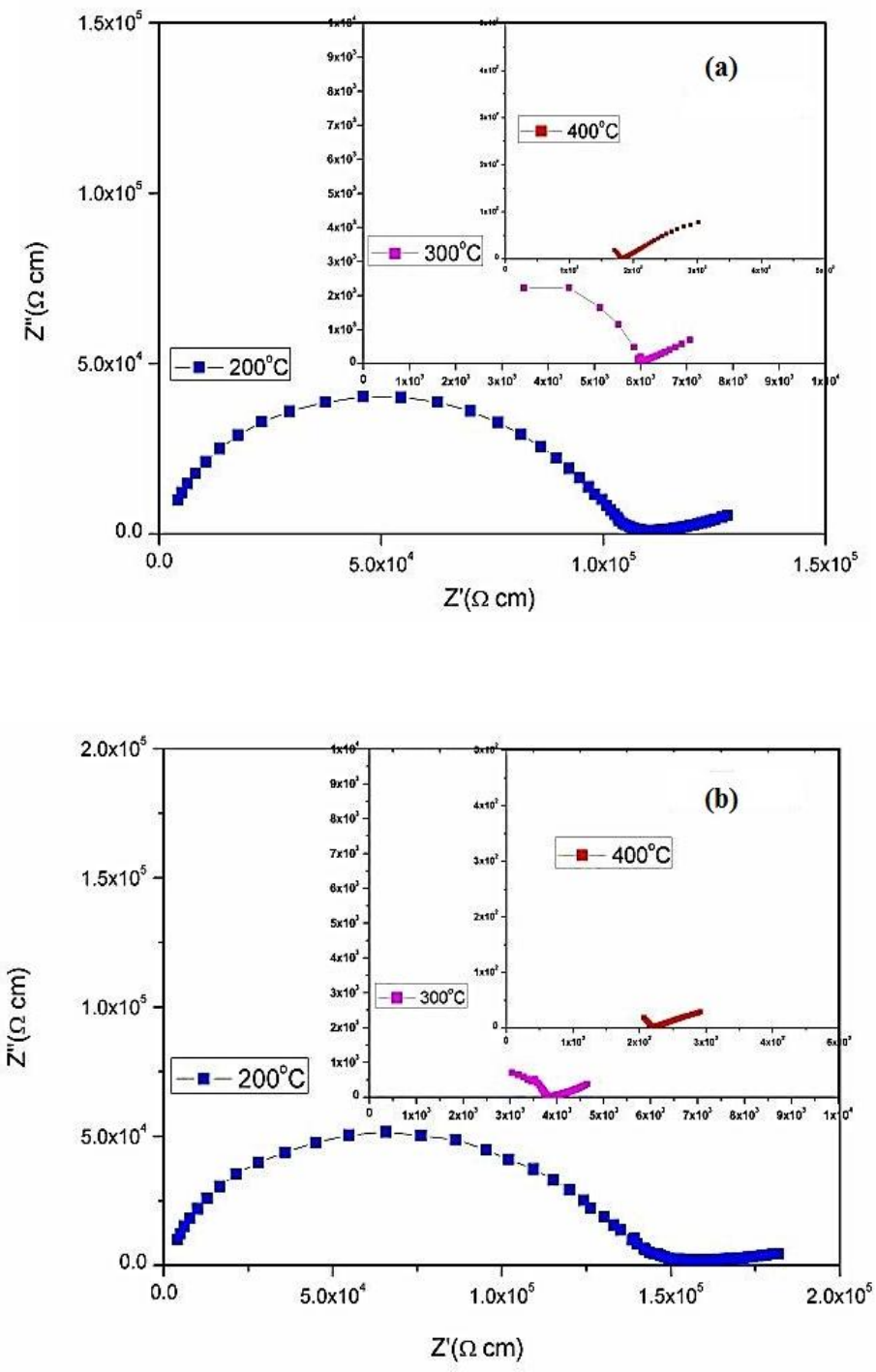

Fig. 5.24: Cole–cole plot for (a) SSR and (b) SCR derived sintered Li_4SiO_4 pellets

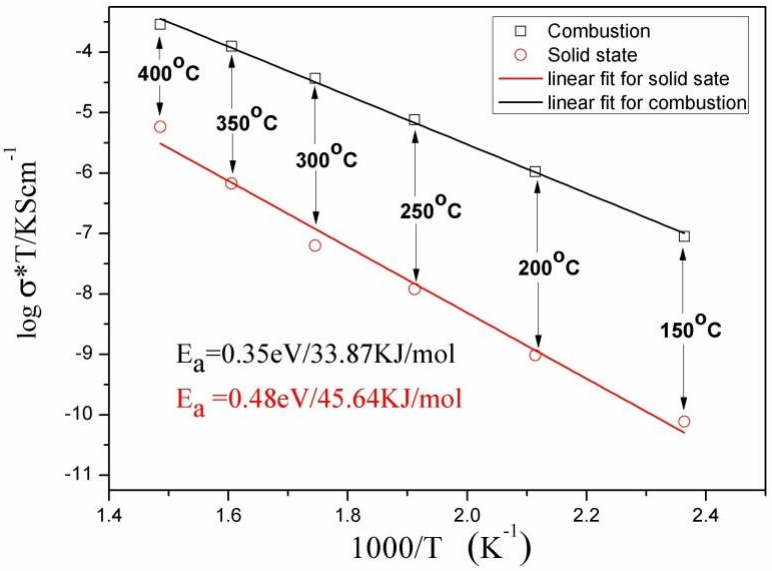

Fig.5.25: Arrhenius plots of the bulk conductivity for the SSR and SCR samples

Fig. 5.25 showed the Arrhenius plots of the bulk conductivity. The bulk conductivity enhanced significantly with the increase of temperature. The SCR sample has smaller grain size compared to SSR sample. The higher conductivity for SCR sample can be ascribed to the enhancement of grain boundary conductivity. Activation energy, $E_a$was found for SCR and SSR sample which came out to be 0.35eV and 0.48eV respectively. It is to be mentioned that the slight difference in activation energy indicating a different conduction mechanism in the solid.

5.15 Thermal conductivity measurement

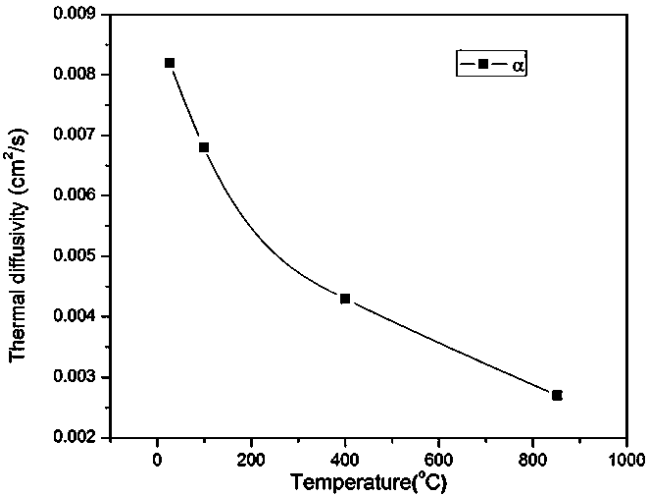

Fig.5.26: Variation of Thermal diffusivity with temperature for SCR samples

The thermal conductivity of cylindrical pellets was determined by the heat pulse method using a laser flash device.Fig.5.26 showed the variation of thermal diffusivity with temperature for sintered SCR pellets. The diffusivity at lower temperature was higher and decreased as the temperature was increased.From the diffusivity data thermal conductivity was been calculated by the formula

$$K_{th} = \alpha C_p \rho \qquad (5.15)$$

Where k_{th} was thermal conductivity in W/m/K, and ρ was the density in Kg/m^3. Heat capacity (C_p) of the solid with temperature was measured simultaneously. The thermal conductivity was calculated to be 2.07 at room temperature and1.42 W/m/K at 400^oC for SCR samples. So it drastically reduces with temperature. Further study is required to understand the behavior. Room temperature thermal conductivity value is better compared to literature reported one [44].

References

[1] S.R. Jain, K.C. Adiga, V.R. Raivernekar, Combust. Flame **40** (1981) 71.

[2] Y.P. Fu, C.C. Chang, C.H. Lin, T.S. Chin, Ceram. Int. **30** (2004) 41.

[3] M. M. Barbooti, A. Dhoaib Al-Sammerrai, ThermochimicaActa, **98**{1}(1986) 119.

[4] X.Wu, Z. Wen, X.Xu, X. Wang, J. Lin, J.Nucl. Mater.**392** (2009) 471.

[5] T. Tang, Z. Zhang, J. Meng, D. Luo, Fusion Eng. Des.**84**{12} (2009) 2124.

[6] J.S.Reed, Principles of ceramic processing, 2nded, John Wiley, (1995) 425-433.

[7] R. F. Speyer, Thermal Analysis of materials, 2nded ,Mercel Dekker, (1993) 35-46.

[8] D. Cruz, S. Bulbulian, E. Lima, and H. Pfeiffer, J. Solid State Chem.**179 {**3}(2006) 909.

[9] G. Mondragon-Gutierrez,D. Cruz,H. Pfeiffer, S.Bulbulian,Res. Lett. Mater. SciArticle ID 908654 (2008) 4.

[10] K.-F. Hesse, Acta Crystallographica B. **33** {3} (1977) 901.

[11] M. J. Venegas, E.Fregoso-Israel, R. Escamilla and H. Pfeiffer, Ind. Eng. Chem. Res.**46** (2007) 2407.

[12] H. Pfeiffer and P. Bosch, Chem. Mater. **17** (2005) 1704.

[13] H. Pfeiffer, K. M. Knowles,J. Eur. Ceram. Soc. **24** (2004) 2433.

[14] D.Cruz, S.Bulbulian, E.Lima,J. Pfeiffer, Solid State Chem.**179** (2006) 909.

[15] C. H.Lu, L. Wei-Cheng, J. Mater. Chem.**10**(2000) 1403.

[16] E.Antolini, M.Ferretti, J. Solid State Chem. **117** (1995) 1.

[17] M. Rahaman, "Ceramic Processing and Sintering", 2nded ,Marcel Dekker, New York, (1995) 470-509.

[18] R. German, Metal Powder Industries Federation, Princeton, NJ (1984).

[19] M. Brown, D. Dolimore, and A. Galwey, Elsevier, Amsterdam, Netherlands, (1980).

[20] A. Galwey and M. Brown, Elsevier, Amsterdam, Netherlands, (1999).

[21] F. Gotor, J. Criado, J. Malek, and N. Koga, J. Phys. Chem.**104** (2000) 777.

[22] E.S. Freeman and B. Carrol, J. Phys. Chem., **62** (1958)397.

[23] J. Frenkel,J. Phys. (Moscow), **5** (1945) 385

[24] M. Rahaman, "Ceramic Processing and Sintering",2nded ,Marcel Dekker, New York, (1995) 153-155.

[25] H. Elbel,J. Nucl. Mater.**155-157** (1988) 480.

[26] T. Hanada, S. Fukada, M. Nishikawa, K. Suematsu, N. Yamashita, T. Kanazawa, Fusion Eng. Des.**85**{7–9} (2010) 998.

[27] N. Roux, S. Tanaka, C. Johnson, R. Verrall, Fusion Eng. Des. **41** (1998) 31.

[28] J. Ortiz-Landeros, L. Martínez-dlCruza, C. Gomez-Yanez, H. Pfeiffer ,ThermochimicaActa**515** (2011) 73.

[29] Z. Xu, J.F.Stebbins, SCIENCE **20**(1995) 1332.

[30] R. Ravikrishna, R. Green and K.T. Valsaraj,J. Sol-Gel Sci. Tech.**34** (2005) 111.

[31] W. T. Hsu, Z. Bin Chen, C. Cheng Wu, R. Kant Choubey and C. Wen Lan, *Nature*:Materials **5** (2012) 227.

[32] H. Yokogawa, M. Yokoyama,J. Non-Cryst. Solids **186** (1995) 23.

[33] Y.-L. Li, Y. Liang, F. Zheng, K. Xiao, Z.Q. Hu,J. Mater Sci. Lett. **14** (1995) 713.

[34] S. Heinze1, B. Vuillemin,P. Giroux,Analusis, **27** (1999) 549.

[35] F. Adam, J. Chua,J. Colloid and Interface Sci.**280** (2004) 55.

[36] C. N. Banwell and E. M. McCash , Fundamentals of molecular spectroscopy, 4thed (1998) 84-88.

[37] A. S. Cavanagh, Y. Lee, B. Yoon, and S. George,E.C.S transaction,**33** {2} (2010) 223.

[38] B. Zhang,M.Nieuwoudtand A. J. Easteal,J. Am. Ceram. Soc.**91**{6} (2008)1927.

[39] J. Serra , P. Gonzalez , S. Liste , C. Serra, S. Chiussi , B. Leon ,M. Perez-Amor, H.O. Ylanen , M. Hupa,J. Non-Cryst. Solids **332** (2003) 20.

[40] J. R. Ferraro, M. H. Manghnani, and L. J. Basile,J. Appl. Phys. **44** (1973)5391.

[41] A.Nakagawa, N. Kuwata, Y. Matsuda and J. Kawamura,J. Phys. Soc. Jpn. **79** (2010) Suppl. A, 98.

[42] Macdonald J.R., Solid State Ionics **25–28** (2005) 1961.

[43] Macdonald J.R. (Ed.), Impedance Spectroscopy Emphasizing Solid Materials and Systems, John Wiley, New York, (1987) 346.

[44] B. Löbbecke , R. Knitter, M. Rohde , J. Reimann, J. Nucl. Mater. **386–388** (2009) 1068.

Chapter 6

Conclusions and Scope of Future Work

6.1 Conclusions

The research work embodied in this dissertation can be divided into three parts. The first part deals with the synthesis of phase-pure Li_4SiO_4 powder using silica prepared from Rice Husk Ash, its compaction behavior and its characterization. The second part deals with the densification study, microstructure analysis, kinetics of initial stage of sintering, Effect of heating rate on density. Third part deals with the porosity analysis and moisture reactivity studies using FTIR analysis studies of electrical conductivity and thermal conductivity on the sintered sample.

1. (a) Li_4SiO_4 powder has been synthesized by solution combustion technique using cheaper precursor of silica i.e. SiO_2 from Rice Husk Ash. White SiO_2 was prepared by several purification treatments from the raw rice husk. Using citric acid as a fuel/complexing agent in controlled amount, Li_4SiO_4 has been synthesized successfully.

(b) It was found that by controlling the citrate to metal ratio, phase pure powder can be found at 650^oC for C/M ratio $\geq$ 1.4. The Φ_e value has been calculated to understand the nature of combustion. Powders were prepared in fuel rich condition. We observed that lower C/M ratio generates impurity phases. The requirement for higher C/M ratio may be due to at low citric acid content chelation was poor and some metal ions like Silicate and Li^+ remains free in the solution. Whereas solid state route (SSR) prepared powder required calcination temperature of 800^oC. In both of the cases Li_4SiO_4 formed via an intermediate phase Li_2SiO_3.The homogenous mixing in the solution phase and presence of citric acid may have favored the formation of Li_2SiO_3 at a lower temperature compared to SSR.The particle size of Li_4SiO_4 powder (prepared by SCR) was found to be around 90 nm and surface area was 2m^2/g. For Li_4SiO_4 powder (prepared by SSR), the particle size and surface area were 0.5-5µm and 1.83m^2/g, respectively. Inductively Coupled Plasma Atomic Emission Spectrometry study shows that 0.13 wt% Al present in the Li_4SiO_4 powder. But it is in allowable limit.

(c) Compaction behavior of Li_4SiO_4 powder prepared by SCR and SSR were analyzed. SCR powder has high density granules with lower agglomerate break point which produce a high compact density.

2.(a) It has been found that SCR derived Li_4SiO_4 powder can be sintered at a temperature as low as 900^oC with a density of 84% of the theoretical density. Li_4SiO_4 SSR powder did not give density above 80% of the theoretical density. Even after trying different sintering arrangements the density could be marginally increased to 85% of the theoretical value for SCR powder. It was seen that the SCR Li_4SiO_4 ceramics showed better microstructure than SSR derived Li_4SiO_4 at 900^oC. The presence of large grain (50 - 100 μm) in SSR could be due to agglomeration whereas in SCR ceramics showed better homogeneity and small size grains (2 - 5 μm).

(b) Kinetic analysis of initial stage of sintering of SCR ceramics revealed that viscous flow sintering mechanisms could be operating with activation energy of 35.8 KJ/mol for the mass transport from bulk grain to neck of the particles. It was seen that the activation energy was independent of the densification rate used for sintering. Optimum heating rate and dwelling period was found out to get maximum density with smaller grain size.

(c) Porosimetry analysis for SSR and SCR pellets were carried out using mercury porosimetry. Macropores of diameter ranging from 0.5 to 200 μm was observed in SSR pellets whereas SCR pellets showed narrow pore size distribution in the range 0.2 – 10 μm. Large and irregular shape grains are reason for wide distribution of porosity in SSR.

(d) FTIR analysis of the moisture exposed SCR powder shows the presence of Li-OH and Si-OH bonds on the surface. Also, long exposure (~ 1 week) of Li_4SiO_4 to moisture environments (95%) forces the breakdown of –Si-O-Si- bond and formation of weaker links of Si-O- bonds with water.

3. (a) Thermal diffusivity was measured by laser flash method. Thermal conductivity value depends on the density and thickness uniformity of the sample.

(b) AC impedance method has been used to characterize electrical property of the sintered sample. SCR derived sample has higher conductivity compared to SSR. The bulk

conductivity enhanced significantly with the increase of temperature. The SCR sample has smaller grain size compared to SSR sample. The higher conductivity for SCR sample can be ascribed to the enhancement of grain boundary conductivity. Activation energy, $E_a$was found for SCR and SSR sample which came out to be 0.35eV and 0.48eV respectively. It is to be mentioned that the slight difference in activation energy indicating a different conduction mechanism in the solid.

6.2 Scope of future work

1. Li_4SiO_4 has high dielectric loss so it can absorb microwave efficiently. Microwave sintering of Li_4SiO_4 ceramics could be done to improve the density above 85% of theoretical value.
2. Pebble formation by extruder spherodizer could be done to achieve better packing density in the breeding blankets.
3. Thermal conductivity of the pebble bed could be found to understand the bed performance.
4. Because of the complexities of the crystal structure of Li_4SiO_4, a detail study of the crystal structure is required using CRYSTAL WARE software. Detailed electrical conductivity study is required.

Publications arising out of M.Tech(R) work

1. **AbhisekChoudhary**, S. Bhattacharyya, P.Chaudhuri, R.Mazumder" Synthesis and sintering of Li_4SiO_4powder from rice husk ash by solution combustion method"(Communicated).
2. **AbhisekChoudhary**, J.P.Nayak, J.Bera, P.Chaudhuri, R.Mazumder "Synthesis of Lithium Orthosilicate by sol-gel Technique: Effect of Two soutce of silica" presented orally in BRFST TOPICAL meeting series and workshop on development of lithium based ceramics for tritium breeding (LCTB-2011) 10-11th June,2011 at NIT Rourkela, Odisha.
3. **AbhisekChoudhary,** B.S.Sahu,P.Chaudhuri, R.Mazumder "Synthesis of Li_4SiO_4 by solution combustion Method for Test Blanket Module Application" presented orally in INTERNATIONAL CONFERENCE on energy efficient materials and Platinum Jubilee session of Indian Ceramic Society on 19-22nd Dec,2011jointly held at Shilpagram, Agra, Uttar Pradesh.
4. **A.Choudhary,** J.Gorinta, B.S. Sahu, P.Adhikari, S.Bhattacharyya, P.Choudhuri,R.Mazumder,"Fabrication and Characterization of Li2TiO3 Pebbles by Extrusion and Spherodization Technique for Test Blanket Module in Fusion Reactor", National Symposium on Materials and Processing-2012(MAP-2012) on 10th-12th Oct, 2012 organized by Materials Research Society of India(Mumbai-Chapter) In association with Bhabha Atomic Research Centre, Mumbai.(**2nd Best Poster Award**) Published in Transaction of Indian Ceramic Society.

Curriculum Vitae

AbhisekChoudhary

S/O Mr. ArbindChoudhary

SinghasiniPalli,Golghar,

Sector-5, Rourkela-769002,

District- Sundergarh, Orissa, INDIA.

Phone No: +91-9338561248 (M)

Email: abhisek.choudhary@gmail.com

Date of Birth: 24.06.1985

Education: M.Sc. (Physics)

Publications/Conference Publications :

1. **AbhisekChoudhary**, S. Bhattacharyya, P.Chaudhuri, R.Mazumder" Synthesis and sintering of Li_4SiO_4powder from rice husk ash by solution combustion method".(Communicated).
2. **AbhisekChoudhary**, J.P.Nayak, J.Bera, P.Chaudhuri, R.Mazumder "Synthesis of Lithium Orthosilicate by sol-gel Technique: Effect of Two soutce of silica" presented orally in BRFST TOPICAL meeting series and workshop on development of lithium based ceramics for tritium breeding (LCTB-2011) 10-11th June,2011 at NIT Rourkela, Odisha.
3. **AbhisekChoudhary,** B.S.Sahu,P.Chaudhuri, R.Mazumder "Synthesis of Li_4SiO_4 by solution combustion Method for Test Blanket Module Application" presented orally in INTERNATIONAL CONFERENCE on energy efficient materials and Platinum Jubilee session of Indian Ceramic Society on 19-22nd Dec,2011jointly held at Shilpagram, Agra, Uttar Pradesh.

Conferences/Workshops attended:

1. **AbhisekChoudhary**, J.P.Nayak, J.Bera, P.Chaudhuri, R.Mazumder "Synthesis of Lithium Orthosilicate by sol-gel Technique: Effect of Two soutce of silica" presented orally in BRFST TOPICAL meeting series and workshop on development of lithium based ceramics for tritium breeding (LCTB-2011) 10-11th June,2011 at NIT Rourkela, Odisha.

2. **AbhisekChoudhary,** B.S.Sahu,P.Chaudhuri, R.Mazumder "Synthesis of Li_4SiO_4 by solution combustion Method for Test Blanket Module Application" presented orally in INTERNATIONAL CONFERENCE on energy efficient materials and Platinum Jubilee session of Indian Ceramic Society on 19-22nd Dec,2011 jointly held at Shilpagram, Agra, Uttar Pradesh.

3. Participated in **INDO-US Workshop** on Functional materials, Processing &Characterization organized by Departemnt of Physics, NIT Rourkela.

4. Participated in 3rd**EICOON SCHOOL** on Science and Technology of Renewable and clean energy sources organized by CSIR-CGCRI and SNBNCBS, Kolkata.

5. J.Gorinta, B.S. Sahu, **A.Choudhary**, P.Adhikari, S.Bhattacharyya, P.Choudhuri,R.Mazumder,"Fabrication and Characterization of Li2TiO3 Pebbles by Extrusion and Spherodization Technique for Test Blanket Module in Fusion Reactor", National Symposium on Materials and Processing-2012(MAP-2012) on 10th-12th Oct, 2012 organized by Materials Research Society of India(Mumbai-Chapter) In association with Bhabha Atomic Research Centre, Mumbai.(**2nd Best Poster Award**) Published in Transaction of Indian Ceramic Society.